Nanomaterials

DOI: 10.1002/anie.200901678

Graphene: The New Two-Dimensional Nanomaterial

C. N. R. Rao, A. K. Sood, K. S. Subrahmanyam, and A. Govindaraj*

Keywords:
carbon · graphene · graphene oxide · monolayers · nanostructures

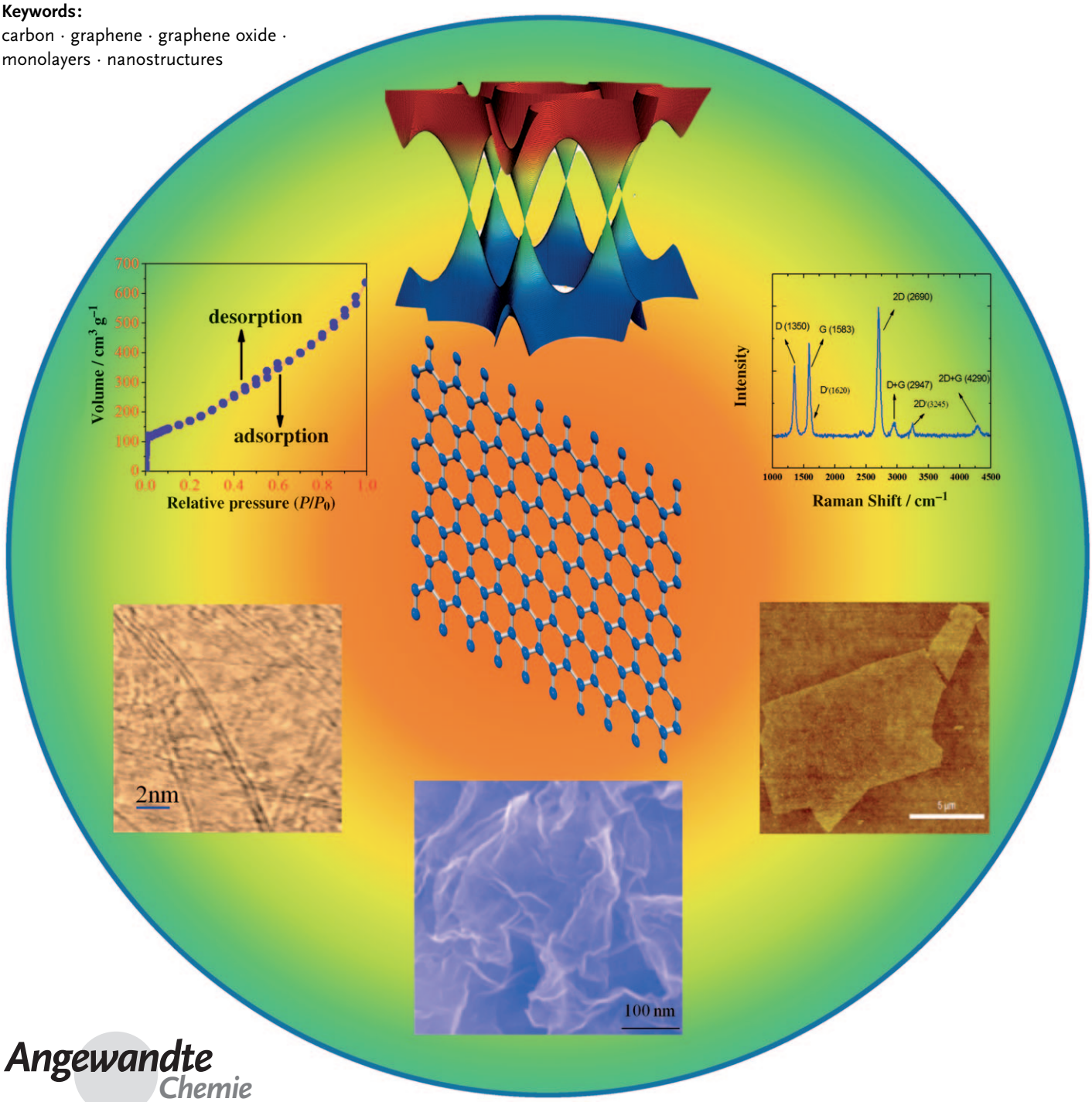

Every few years, a new material with unique properties emerges and fascinates the scientific community, typical recent examples being high-temperature superconductors and carbon nanotubes. Graphene is the latest sensation with unusual properties, such as half-integer quantum Hall effect and ballistic electron transport. This two-dimensional material which is the parent of all graphitic carbon forms is strictly expected to comprise a single layer, but there is considerable interest in investigating two-layer and few-layer graphenes as well. Synthesis and characterization of graphenes pose challenges, but there has been considerable progress in the last year or so. Herein, we present the status of graphene research which includes aspects related to synthesis, characterization, structure, and properties.

From the Contents

1. Introduction

Graphene, the parent of all graphitic forms (Figure 1), has become one of the most exciting topics of research in the last three to four years.[1] This two-dimensional material constitutes a new nanocarbon comprising layers of carbon atoms arranged in six-membered rings. It is distinctly different from carbon nanotubes (CNTs) and fullerenes, and exhibits unique properties which have fascinated the scientific community. Typically important properties of graphene are a quantum Hall effect at room temperature,[2–4] an ambipolar electric field effect along with ballistic conduction of charge carriers,[5] tunable band gap,[6] and high elasticity.[7] Although graphene is expected to be perfectly flat, ripples occur because of thermal fluctuations.[1] Ideally graphene is a single-layer material, but graphene samples with two or more layers are being investigated with equal interest. Three different types of graphenes can be defined: single-layer graphene (SG), bilayer graphene (BG), and few-layer graphene (FG, number of layers ≤ 10). Although single-layer graphene and bilayer graphene were first obtained by micro-mechanical cleavage,[5] several strategies have since been developed for the synthesis of graphenes.[8]

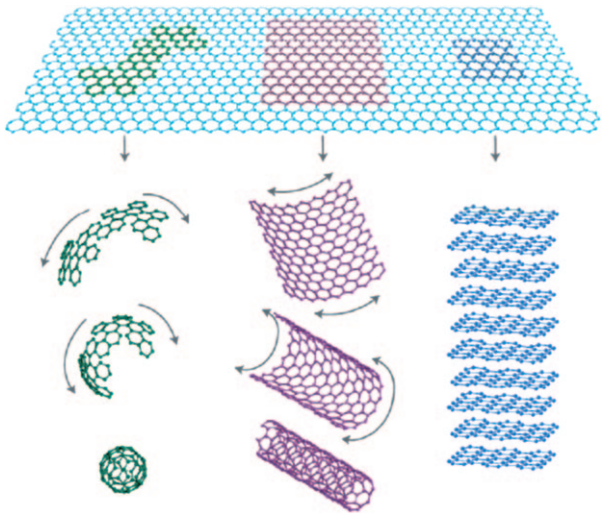

Figure 1. Graphene: the parent of all graphitic forms. (From Ref. [1a].)

Graphene has been characterized by a variety of microscopic and other physical techniques including atomic force microscopy (AFM), transmission electron microscopy (TEM), scanning tunneling microscopy (STM), X-ray diffraction (XRD), and Raman spectroscopy.[1] It is interesting that single-layer graphene placed on a silicon wafer with a 300 nm thick layer of SiO_2, becomes visible in an optical microscope (Figure 2a and b).[8–10] While AFM directly gives the number of layers (Figure 2c),[8] STM (Figure 2d)[11] and TEM (Figure 2e)[12] images are useful in determining the morphology and structure of graphene. Raman spectroscopy has emerged to be an important tool for the characterization of graphene samples.[13–16] Herein, we shall discuss various aspects of graphene, including synthesis, structure, properties, functionalization, and polymer composites. Although we have covered most of the important facets of graphene published up to May 2009, we have given somewhat greater importance to the chemical aspects and cited a large number of references from the rapidly increasing literature. We do hope that the

[*] Prof. Dr. C. N. R. Rao, K. S. Subrahmanyam, Dr. A. Govindaraj
International Centre for Materials Science, New Chemistry Unit and CSIR Centre of Excellence in Chemistry, Jawaharlal Nehru Centre for Advanced Scientific Research
Jakkur P. O., Bangalore 560 064 (India)
Fax: (+91) 80-2208-2760
E-mail: cnrrao@jncasr.ac.in
Prof. Dr. A. K. Sood
Department of Physics, Indian Institute of Science
Bangalore 560 012 (India)

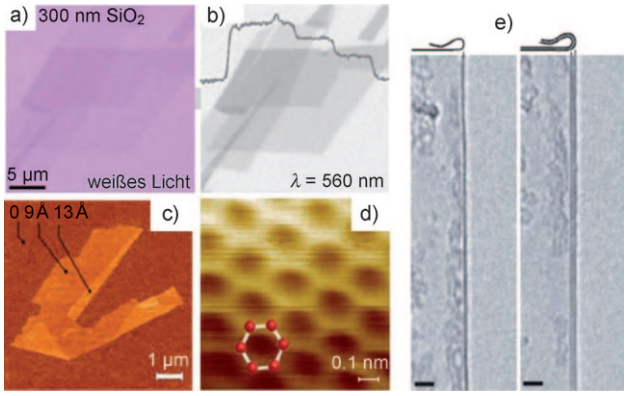

Figure 2. Microscopy images of graphene crystallites on 300 nm SiO_2 imaged with a) white and b) green light. Figure (b) shows step-like changes in the contrast for single-, bi-, and trilayer graphenes. c) AFM image of single-layer graphene. The folded edge exhibits a relative height of approximately 4 Å indicating that it is single-layer. d) High-resolution STM image. e) TEM images of folded edges of single- and bilayer graphenes. (From Refs. [9, 11, 12b].)

references are sufficiently representative and will help the reader to obtain more detailed information.

2. Synthesis

2.1. Single-Layer Graphene

Single-layer graphene has been generally prepared by micromechanical cleavage in which highly oriented pyrolitic graphite (HOPG) is pealed using scotch-tape and deposited on to a silicon substrate. Besides mechanical cleavage of graphite, the other important methods employed to produce graphene samples are epitaxial growth on an insulator surface (such as SiC), chemical vapor deposition (CVD) on the surfaces of single crystals of metals (e.g., Ni), arc discharge of graphite under suitable conditions, use of intercalated graphite as the starting material, preparation of appropriate colloidal suspensions in selected solvents, and reduction of graphene oxide sheets.[8]

By employing mechanical exfoliation of graphite, monolayers and bilayers of graphene with minimum lateral dimensions of 2–10 nm can be deposited onto the Si(100)-2×1:H surface.[17] Room-temperature ultrahigh vacuum scanning tunneling spectroscopy has been used to characterize the nanometer-sized single-layer graphene to reveal a size-dependent energy gap ranging from 0.1 to 1 eV. By correlating resolved tunneling spectroscope and atomically resolved images, the dependence of the electronic structure of single-layer graphene on lateral size, edge structure, and crystallographic orientation has been examined. Single- and few-layer graphenes taken from freshly cleaved HOPG surfaces by the scotch-tape technique can be readily transferred on to a given substrate using electrostatic deposition.[18]

While mechanical cleavage of graphene layers from a graphite crystal has afforded the study of the properties of single-layer graphene or bilayer graphene, the method is not suitable for large scale synthesis of single-layer graphene or of few-layer graphene (FG). Among the methods and procedures for large-scale synthesis two categories should be distinguished: a) those which start with graphite or a comparable starting material not containing any oxygen function-

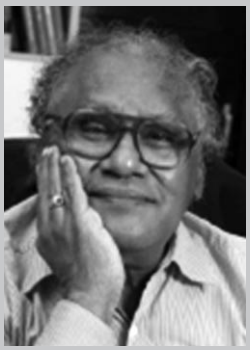

C. N. R. Rao *obtained his PhD degree from Purdue University (1958) and DSc degree from the University of Mysore (1961). He is the National Research Professor and Linus Pauling Research Professor at the Jawaharlal Nehru Centre for Advanced Scientific Research and Honorary Professor at the Indian Institute of Science (both at Bangalore). His research interests are mainly in the chemistry of materials. He is the recipient of the Einstein Gold Medal of the UNESCO, the Hughes Medal of the Royal Society, and the Somiya Award of the International Union of Materials Research Societies (IUMRS). In 2005, he received the Dan David Prize for materials research and the first India Science Prize.*

K. S. Subrahmanyam *received his MSc (Chemistry) degree from University of Hyderabad in 2006. He is a student of PhD programme in the Jawaharlal Nehru Centre for Advanced Scientific Research, Bangalore and received his MS (Engg.) degree in 2008. He is working on synthesis and characterization of graphenes.*

A. K. Sood *is a Professor of Physics at the Indian Institute of Science, Bangalore. He is a member of the science academies of India and has received various medals and honours in physics including the Bhatnagar Prize and the TWAS Prize. His main interests are soft condensed matter, nanomaterials, and light scattering.*

A. Govindaraj *obtained his PhD degree from University of Mysore and is a Senior Scientific Officer at the Indian Institute of Science, and Honorary Faculty Fellow at the Jawaharlal Nehru Centre for Advanced Scientific Research. He works on different types of nanomaterials. He has authored more than 100 research papers and co-authored a book on nanotubes and nanowires.*

alities and b) those which involve the exfoliation of graphite oxide (GO) followed by reduction. The latter methods yield sheets of reduced graphite oxide, some of which could be single-layer materials. Reduced graphite oxide layers are to be considered as chemically modified graphenes since they generally contain some oxygen functions, such as OH or COOH groups. Under category (a), some of the methods are growth on SiC surfaces, hydrogen arc discharge, conversion of nanodiamond, CVD on metal surfaces, and dispersion of graphite in solvents.

Large-area single-layer graphene has been prepared by thermal decomposition of the (0001) face of a 6H-SiC wafer under ultrahigh vacuum (UHV) conditions.[19] Single-layer graphene has been grown on top of a 6H-SiC (0001) substrate by an ex situ method, which gives larger mono-layer graphenes in comparison with an in situ method (Figure 3).[20a] Thus, ex situ graphitization of Si-terminated SiC (0001) in an argon atmosphere of 1 bar yields monolayer films with large domain sizes.[20b] Temperature-dependent structural changes of graphene layers on the 6H-SiC(0001) surface studied by photoelectron spectroscopy, low-energy electron diffraction, and extended X-ray absorption spectroscopy (EXAFS) indicate that a bilayer-like graphene sheet is formed after annealing at 1150 °C. The tilting angle of the graphene sheet is estimated to be $14 \pm 2°$. As the number of the graphene layers increases, the angle gradually decreases to $7 \pm 2°$ at 1400 °C.[20c]

Graphene suspensions can be readily produced by dispersing graphite in surfactant–water solutions.[21a] Individual sheets on HOPG have been manipulated by scanning probe microscope (SPM) tips, but it is more reliable to first pattern the HOPG surface to create an array of small graphite islands by reactive ion etching with an oxygen plasma.[21b] Exfoliation of lithium-intercalated multiwalled carbon nanotubes yields single-layer graphene flakes.[22a]

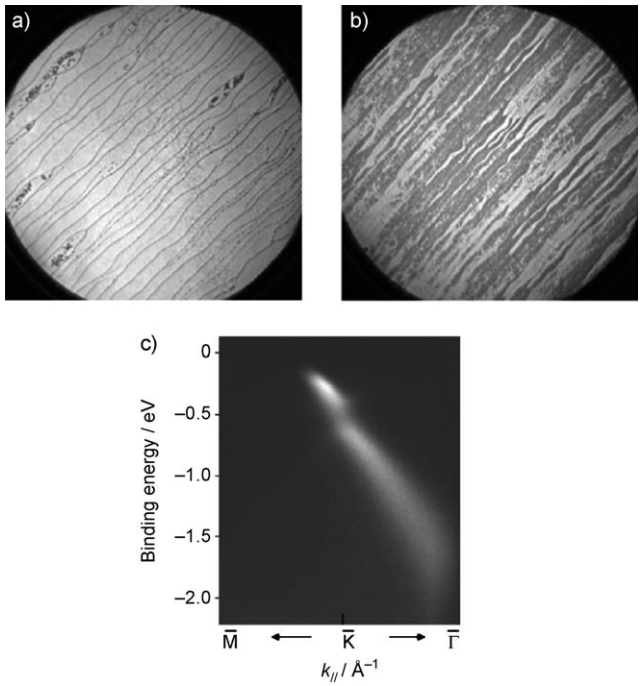

Figure 3. a) Low-energy electron microscope (LEEM) image of a single-domain single-layer graphene grown ex situ on the (0001) surface of SiC; the field of view is 20 μm wide and the electron energy is $E_{vac} + 4.4$ eV. b) LEEM image showing the existence of two domains of monolayer graphene. c) Photoelectron intensity map versus binding energy and parallel momentum showing the electronic structure close to the Dirac point at the *K* point of the Brillouin zone. (From Ref. [20a].)

Gram quantities of single-layer graphene have been prepared by employing a solvothermal procedure and subsequent by sonication.[23] In this process, the solvothermal

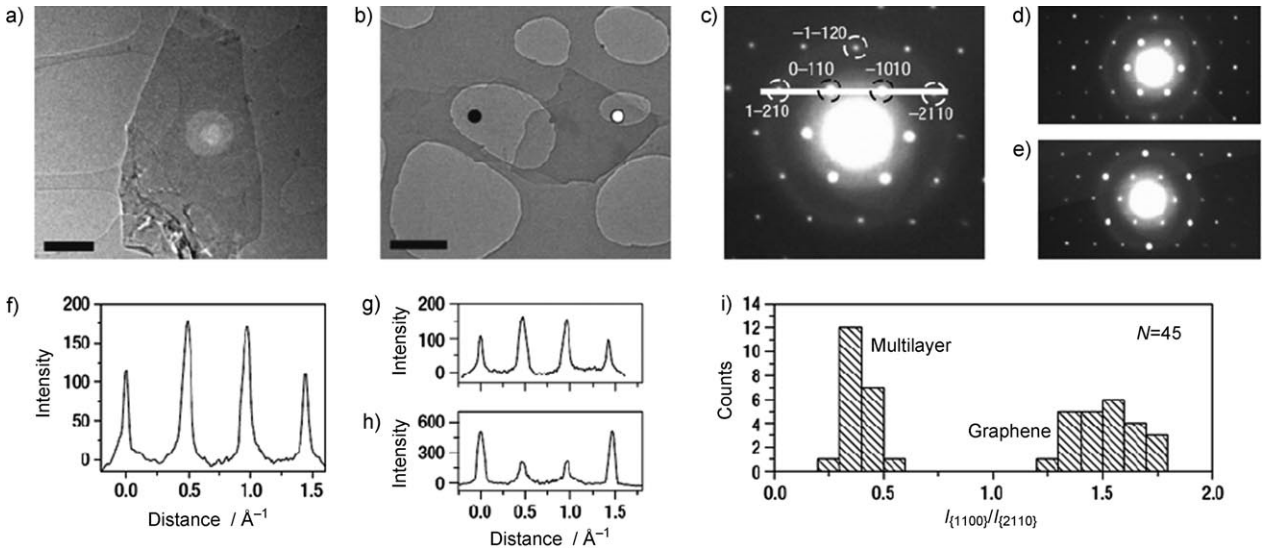

Figure 4. a,b) High-resolution TEM images of a) solution-cast monolayer and b) solution-cast bilayer graphenes (scale bar 500 nm). c) Electron diffraction pattern of the monolayer in (a). d,e) Electron diffraction patterns taken from the positions of the d) black and e) white spots, respectively, of the sheet in (b). The graphene is one-layer thick in (d) and a bilayer in (e). f–h) Diffracted intensity taken along the 1−210 to −2110 axis for the patterns in (c–e). i) Histogram of the ratios of the intensity of the {1100} and {2110} diffraction peaks. A ratio >1 is a signature of graphene. (From Ref. [24].)

product of sodium and ethanol is subjected to low-temperature flash pyrolysis yielding a fused array of graphene sheets, which are dispersed by mild sonication. Single-layer graphene can be produced in good yields by solution-phase exfoliation of graphite in an organic solvent, such as *N*-methylpyrrolidone (NMP) (Figure 4).[24] This process works because the energy required to exfoliate graphene is balanced by the solvent–graphene interaction. Exfoliation of alkali-metal intercalated graphite in NMP yields a stable solution of negatively charged graphene sheets which can be deposited on substrates.[25] Two-dimensional linear graphene ribbons can be prepared chemically by the oxidative cyclodehydrogenation of polyphenylene precursors.[26]

Highly conducting graphene sheets produced by the exfoliation–reintercalation–expansion of graphite are readily suspended in organic solvents.[27] The sheets in organic solvents can be made into large, transparent, conducting films by Langmuir–Blodgett assembly in a layer-by-layer manner. The initial step is exfoliation of the commercial expandable graphite (160–50 N, Grafguard) by brief (60 s) heating to 1000 °C in forming gas (i.e. hydrogen and nitrogen), followed by reintercalation by oleum (fuming sulfuric acid with 20 % free SO_3), and insertion of tetrabutylammonium hydroxide (TBA, 40 % solution in water) into the oleum-intercalated graphite in DMF. TBA-inserted oleum-intercalated graphite is sonicated in a DMF solution of 1,2-distearoyl-*sn*-glycero-3-phosphoethanolamine-*N*-[methoxy-(polyethyleneglycol)-5000] (DSPE-mPEG) for 60 min to obtain a homogeneous suspension. This method gives large amounts of graphene sheets which can be transferred to other solvents including water and organic solvents (Figure 5). The average size of the single-layer graphene sheet was 250 nm and the average topographic height was approximately 1 nm. Graphitic oxide, obtained by the oxidation of graphite, contains a considerable amount of surface oxygen in the form of OH and COOH groups. Mechanical or thermal exfoliation graphitic oxide gives single-layer graphene oxide (SGO). Single-layer graphene oxide on reduction by hydrogen, hydrazine or other reducing agents gives single-layer graphene. Single-layer graphene has been prepared on a large scale by a solution-based approach, involving the dispersion of graphitic oxide in pure hydrazine. Hydrazine-based

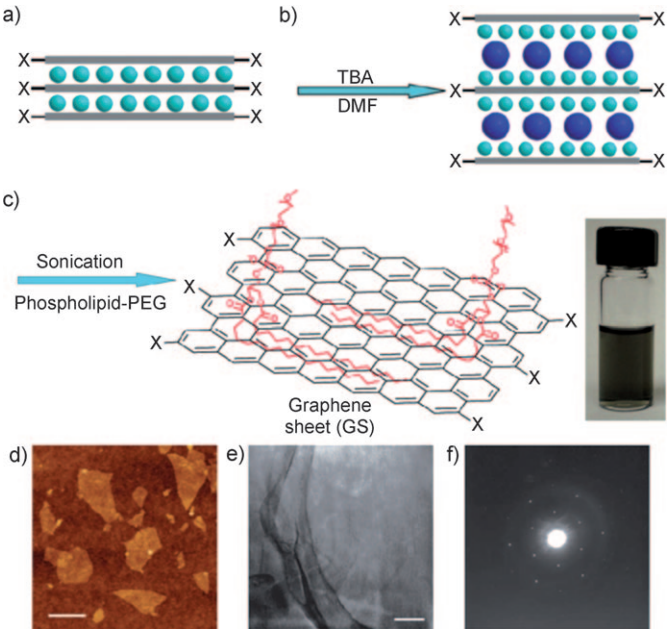

Figure 5. a) Schematic representation of the exfoliated graphite reintercalated with sulphuric acid molecules (spheres) between the layers. b) Schematic of tetrabutyl ammoniumhydroxide (TBA; dark blue spheres) in the intercalated graphite. c) Schematic of single-layer graphene coated with DSPE–mPEG molecules also shown is a photograph of the solution of single-layer graphene. d) AFM image of a single-layer graphene with a topographic height of approximately 1 nm (scale bar: 300 nm. e) Low-magnification TEM image of a single-layer graphene that is several hundred nanometres in size (scale bar: 100 nm). f) Electron diffraction pattern of a single-layer graphene as in (e). (From Ref. [27].)

colloids are deposited on different substrates to obtain chemically modified graphene sheets with large areas (20 × 40 μm; Figure 6).[29a] Schniepp et al.[29b] have shown that exfoliation of graphitic oxide yields single-layer graphene oxide through the expansion of CO_2 evolved in the space between the sheets during rapid heating (Figure 7). A detailed analysis of the thermal-expansion mechanism of graphitic oxide to produce single-layer graphene sheets has been described.[29c] Chemically modified graphenes have been produced in different ways. These include hydrazine reduc-

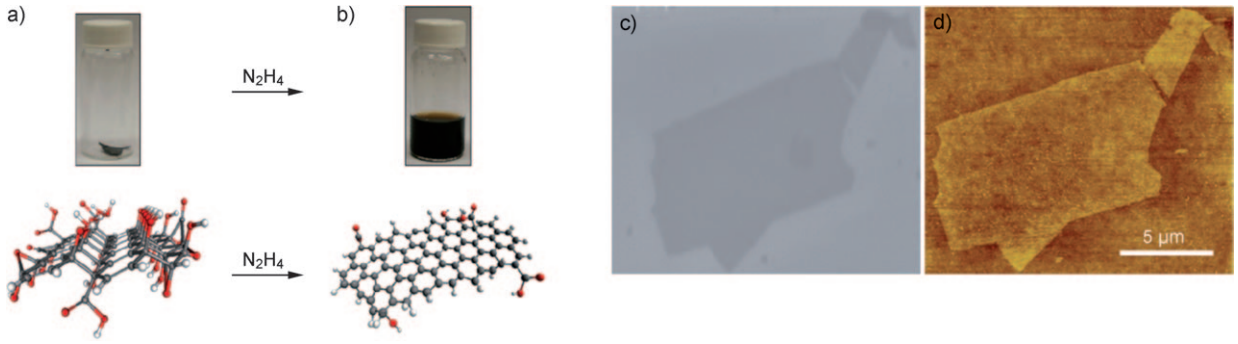

Figure 6. Photographs of chemically converted graphene suspensions. a) graphite oxide paper in a glass vial and b) the graphite oxide dispersion after addition of hydrazine. Below the vials, three-dimensional computer-generated molecular models of graphene oxide (C gray, O red, H white) and the reduced graphene are shown. Removal of -OH and -COOH groups by reduction gives the planar structure. c) SEM and d) AFM images of a chemically converted graphene sheet on Si/SiO_2 substrate. (From Ref. [29a].)

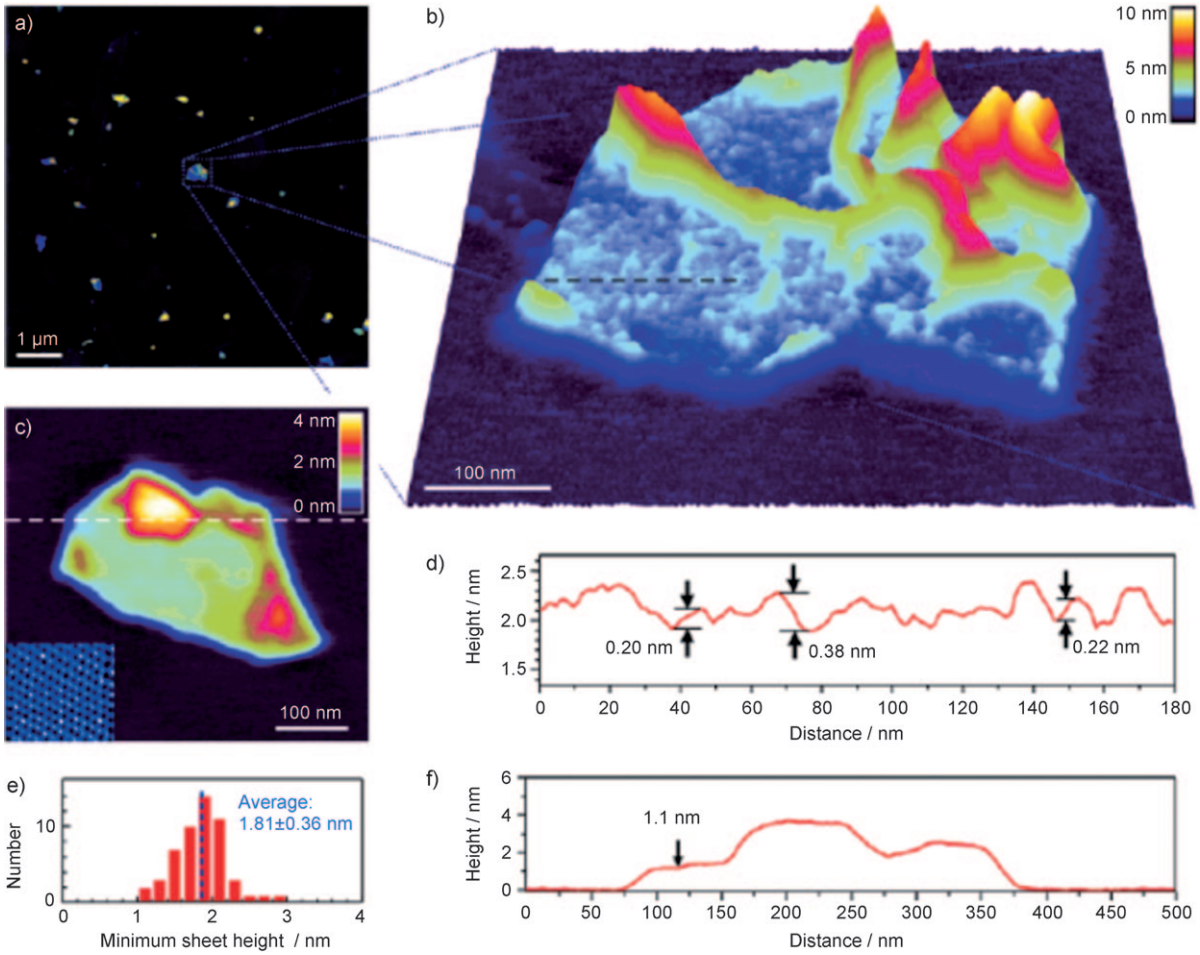

Figure 7. a) Tapping-mode AFM image (8 μm × 8 μm) showing an individual thermally exfoliated graphite oxide flakes. b) Pseudo-3D representation of a 600 nm × 600 nm AFM scan of an individual graphene sheet showing the wrinkled, rough surface. c) Contact-mode AFM scan of a different flake, providing an accurate thickness of the sheet. Inset: atomic-scale image of the HOPG lattice. d) Cross-section of an unwrinkled area in (b) (position indicated by black dashed line in (b)). e) Histogram showing the narrow distribution of sheet heights. f) Cross-section through the sheet in (c) showing a height minimum of 1.1 nm. (From Ref. [29b].)

tion of the colloidal suspension of single-layer graphene oxide in DMF/water[28a] or in water.[28b] Electrostatic stabilization enables stable aqueous dispersions of the single-layer graphene sheets.

2.2. Graphenes with One to Three Layers

The dispersion behavior of graphene oxide in different organic solvents, such as DMF, NMP, ethylene glycol and tetrahydrofuran (THF) has been studied.[30] As-prepared graphite oxide formed by the Hummers method undergoes full exfoliation into single-layer graphene oxide under sonication forming stable dispersions in the above solvents. The sample prepared from the dispersion in DMF yields sheets of uniform thickness (1.0–1.4 nm). Single-layer and bilayer graphene sheets are obtained by using a substrate-free, atmospheric-pressure microwave plasma reactor, wherein liquid ethanol droplets are passed through an argon plasma (Figure 8).[31] High-quality graphene sheets of 1–3 layers have been synthesized on stainless steel substrates at 500 °C by microwave plasma chemical vapor deposition (CVD) in an atmosphere of 10 % methane and 90 % hydrogen at a pressure of 30 torr and a flow rate of 200 sccm (standard cubic centimeter per minute).[32] Arc-discharge of graphite in hydrogen appears to yield primarily two- and three-layer graphenes (see next section).

2.3. Few-Layer Graphenes

Starting with graphite and by employing chemical exfoliation, high-quality graphene with a predetermined number of layers can be obtained.[33] With artificial graphite, flake graphite powder, Kish graphite, and natural flake graphite as starting materials, nearly 80 % of the final product has been found to be single-layer, single- and double-layer, double- and triple-layer, and few-layer (4–10 layers) graphene respectively. A mixture of few-layer (4–10 layers) graphene and thick graphene (> 10 layers) is obtained when HOPG is used (Figure 9). Large-scale transfer of mono and few-layer graphenes from SiO_2/Si, to any type of substrate material

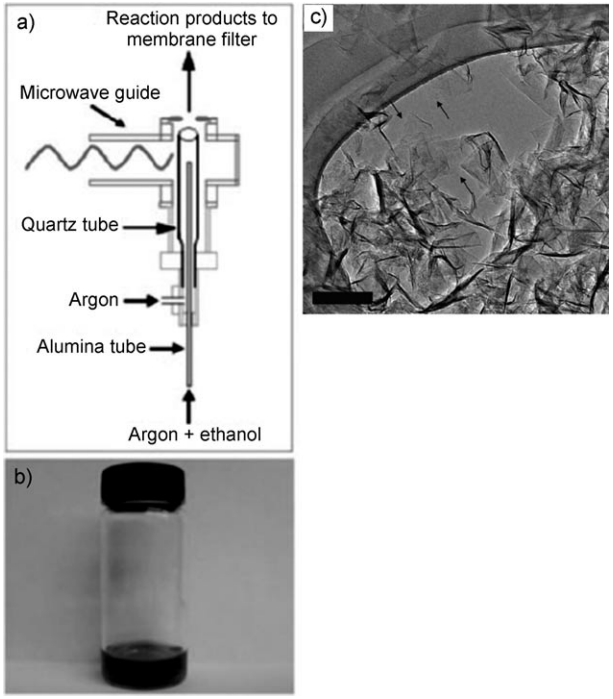

Figure 8. Synthesis of graphene sheets: a) Schematic representation of the atmospheric-pressure microwave plasma reactor. b) Photograph of graphene sheets dispersed in methanol. c) TEM image of graphene sheets suspended on a carbon TEM grid. Homogeneous and featureless regions (indicated by arrows) indicate areas of single-layer graphene; Scale bar: 100 nm. (From Ref. [31].)

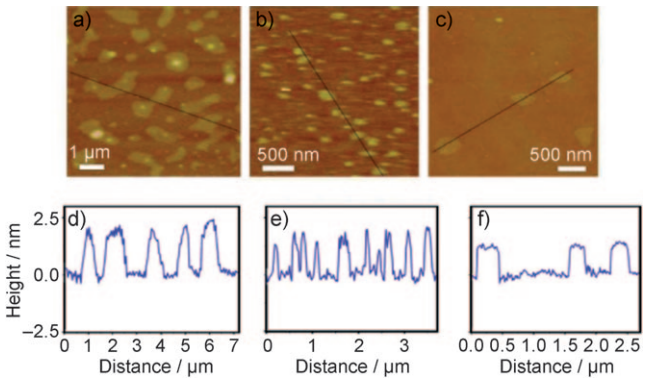

Figure 9. Tapping-mode AFM images and the height profiles of graphenes derived from a),d) kish graphite, b),e) flake graphite powder, and c),f) artifical graphite. The thickness of the graphenes are 1.9–2.3 nm, 1.3–2.1 nm, and 1.1–1.3 nm respectively. (From Ref. [33].)

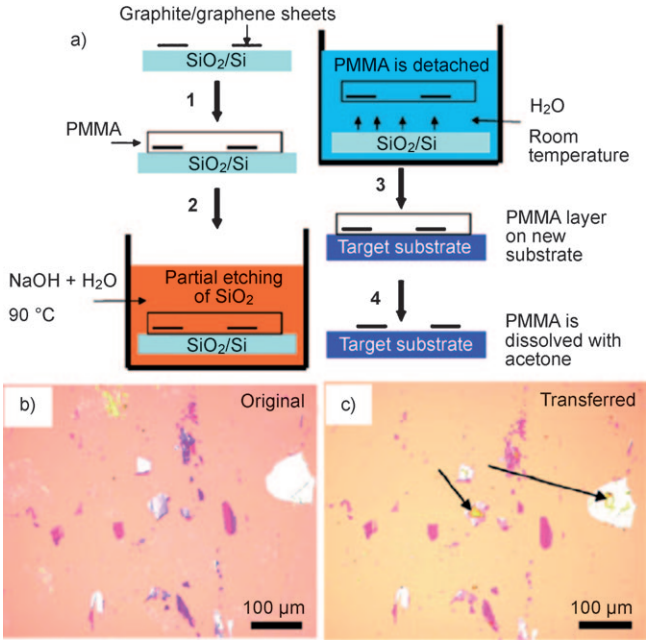

Figure 10. a) Schematic representation of the transferring process. Graphene sheets are deposited on SiO_2/Si substrates via HOPG microcleaving and then transferred to a nonspecific substrate. b,c) Optical images of macroscopic regions having graphite and graphene flakes on b) the original substrate and c) the SiO_2/Si substrates. Arrows point to PMMA residues. (From Ref. [34].)

has been carried out. During the transferring process no morphological changes or corrugations are induced (Figure 10).[34] Well-ordered graphite films with a thickness of a few graphene layers have been grown on nickel substrates by CVD from a mixture of hydrogen and methane activated by a direct current (DC) discharge.[35] These films contain atomically smooth micron-size regions separated from each other by ridges. The film thickness is (1.5 ± 0.5) nm.

An arc-discharge method involving evaporation of graphite electrodes in a hydrogen atmosphere has been reported for preparing graphene flakes.[36a] The presence of H_2 during the arc-discharge process terminates the dangling carbon bonds with hydrogen and prevents the formation of closed structures, [37–38] such as rolling of sheets into nanotubes and graphitic polyhedral particles. This method is useful to prepare boron- and nitrogen-doped graphene. To prepare pure graphene (HG), direct current arc evaporation of graphite was carried out in a water-cooled stainless steel chamber filled with a mixture of hydrogen and helium in different proportions, without using a catalyst. The proportions of H_2 and He used in our experiments are, H_2 (70 torr)/He (500 torr), H_2 (100 torr)/He (500 torr), H_2 (200 torr)/He (500 torr), and H_2 (400 torr)/He (300 torr). In a typical experiment, the discharge current was in the 100–150 A range, with a maximum open circuit voltage of 60 V.[39] The arc was maintained by continuously translating the cathode to keep a constant distance of 2 mm from the anode. The arc discharge deposit formed on the inner walls of the reaction chamber was examined to characterize the graphene (Figure 11). The deposit mainly contained graphenes with 2–4 layers and the areas were in the $10–40 \times 10^3$ nm^2 range. Hydrogen arc discharge of graphitic oxide has also been employed to produce graphene sheets.[36b]

Using microwave plasma-enhanced CVD, under a flow of a methane/hydrogen mixture, micrometer-wide flakes consisting of few-layer graphene sheets (four to six atomic layers) have been prepared on quartz and silicon by the controlled recombination of carbon radicals in the microwave plasma.[40] Continuous large-area films of single- to few-layer graphene have been grown on polycrystalline Ni films by ambient-pressure CVD using methane/hydrogen feed gas and trans-

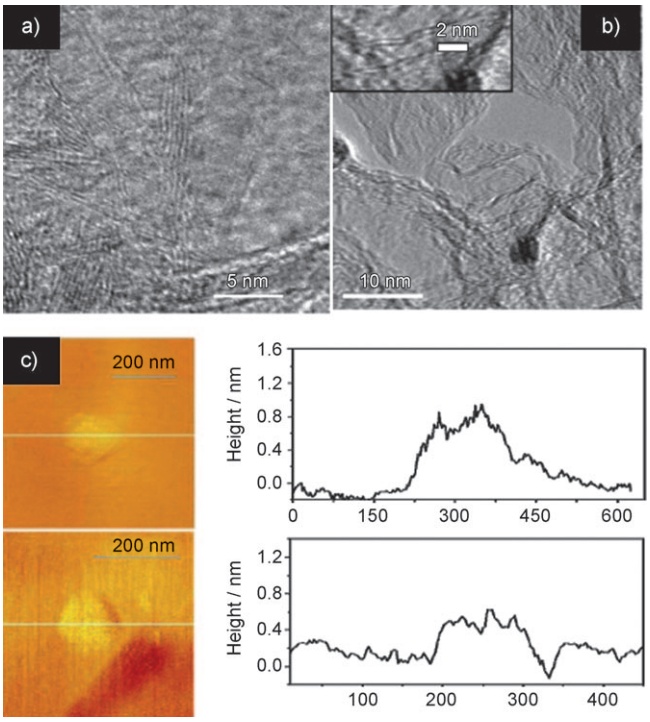

Figure 11. a,b) High resolution TEM images of graphene (HG) prepared by the arc-discharge method (inset in (b) shows clearly a bi-layer graphene). c) AFM images and height profiles (1–2 layers). (From Ref. [36a].)

ferred on to substrates assisted by poly(methyl methacrylate) wet etching (Figure 12).[41] Highly crystalline graphene ribbons (< 20–30 μm in length) with widths of 20–300 nm and a small thickness (2–40 layers) have been synthesized by aerosol pyrolysis using a mixture of ferrocene, thiophene, and ethanol.[42] A microwave plasma enhanced CVD strategy, also called a substrate-lift-up approach, has been used for the efficient synthesis of multilayer graphene nanoflake films on Si substrates without the use of metal catalysts.[43]

Single- and few-layer graphene films exhibiting electrical characteristics somewhat similar to bilayer graphene have been deposited onto Si/SiO_2 substrates starting from graphitic oxide.[44] Stable dispersions of graphitic oxide in a mixture of water and a non-aqueous solvent such as DMF, methanol, or acetone, are spray deposited on a pre-heated substrate,

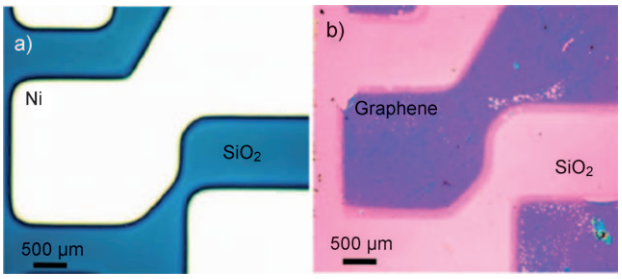

Figure 12. a) Optical image of a prepatterned nickel film on SiO_2/Si. CVD graphene is grown on the surface of the nickel pattern. b) Optical image of the grown graphene transferred from the nickel surface in panel (a) to another SiO_2/Si substrate. (From Ref. [41].)

subsequent chemical reduction yields non-agglomerated graphene sheets. Stable aqueous dispersions of single to few-layer graphene sheets have been prepared using a water soluble pyrene derivative (1-pyrenebutyrate) as the stabilizer and hydrazine monohydrate as the reducing agent.[45] Since the pyrene moiety has strong affinity (because of π-stacking) with the basal plane of graphite, the flexible graphene sheets become non-covalently functionalized. Few-layer graphene nanosheets can also be produced by a soft chemistry route involving graphite oxidation, ultrasonic exfoliation, and chemical reduction by refluxing with hydroquinone.[46]

Chemical vapor deposition using camphor (camphor graphene; CG), conversion of nanodiamond (nanodiamond graphene; DG) and thermal exfoliation of graphitic oxide (exfolitated graphitic oxide graphene; EG) produce few-layer graphenes in large quantities.[47] In the first method, camphor is pyrolysed over nickel nanoparticles at 770 °C in the presence of argon.[48] The method to prepare DG involves annealing nanodiamond at 1650 °C or higher in a helium atmosphere.[49] It is generally found that the surface areas vary as EG > DG > HG. The number of layers is smallest (2–4) in HG. Large and flat graphene flakes having single to few layers have been produced from HOPG by an initial epoxy bonding process followed by reverse exfoliation.[50] Kim et al[51a] have carried out large-scale growth of graphene films by CVD on thin nickel layers (< 300 nm) deposited on SiO_2/Si substrates.[51a] These workers also describe two methods of patterning the films and transferring them on to substrates (Figure 13). The reaction of $CH_4/H_2/Ar$ is carried out at 1000 °C. ^{13}C labeled graphene has been prepared by CVD of $^{13}CH_4$ over nickel foil.[51b] Layer-by-layer growth of graphene on Ru-(0001) has been accomplished by temperature annealing of the metal containing interstitial carbon atoms[51c,d] Films of giant graphene molecules such as $C_{42}H_{18}$ and $C_{96}H_{30}$ have been processed through soft-landing mass spectroscopy.[51e]

Preparation and characterization of graphene oxide paper, a free-standing carbon-based membrane material made by flow-directed assembly of individual graphene oxide sheets has been reported (Figure 14).[52] In this procedure, graphite oxide synthesized by the Hummers method was dispersed in water as individual graphene oxide sheets and the graphene oxide paper was made by filtration of the resulting colloid through an Anodisc membrane filter (47 mm diameter, 0.2 μm pore size; Whatman), followed by air drying and peeling from the filter.

While the exact procedures for large-scale synthesis of graphenes, specially single-layer graphene and few-layer graphene (with a relatively small number of layers, ≤ 6) have not been established, the most popular method appears to be one based on graphite oxide. Graphite oxide itself is prepared by treating graphite with a mixture of concentrated nitric acid, concentrated sulfuric acid, and potassium chlorate at room temperature for five days.[53] Exfoliation is carried out by giving a sudden thermal shock to graphitic oxide in a long quartz tube at 1050 °C under an argon atmosphere.[23] A stable suspension can be prepared by heating an exfoliated graphite oxide suspension under strongly alkaline conditions at moderate temperatures (50–90 °C).[54] Chemical reduction of exfoliated graphite oxide by reducing agents, such as hydra-

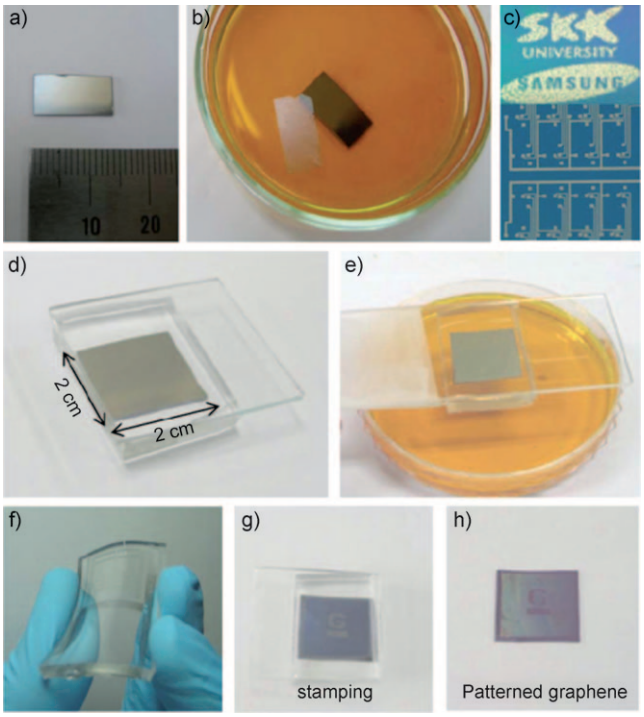

Figure 13. Transfer processes for large-scale graphene films. a) Graphene film (centimetre-scale) grown on a Ni (300 nm)/SiO2 (300 nm)/Si substrate, b) after etching the nickel layers in 1 M $FeCl_3$ aqueous solution. c) Graphene films having different shapes can be synthesized on top of patterned nickel layers. d, e) The dry-transfer method using a polydimethylsiloxane (PDMS) stamp is useful in transferring the patterned graphene films. d) the graphene film on the PDMS substrate, e) the underlying nickel layer is etched away using $FeCl_3$ solution. f) Transparent and flexible graphene films on the PDMS substrates. g,h) The PDMS stamp makes conformal contact with a SiO_2 substrate. Peeling back the stamp (g) leaves the film on a SiO_2 substrate (h). (From Ref. [51a].)

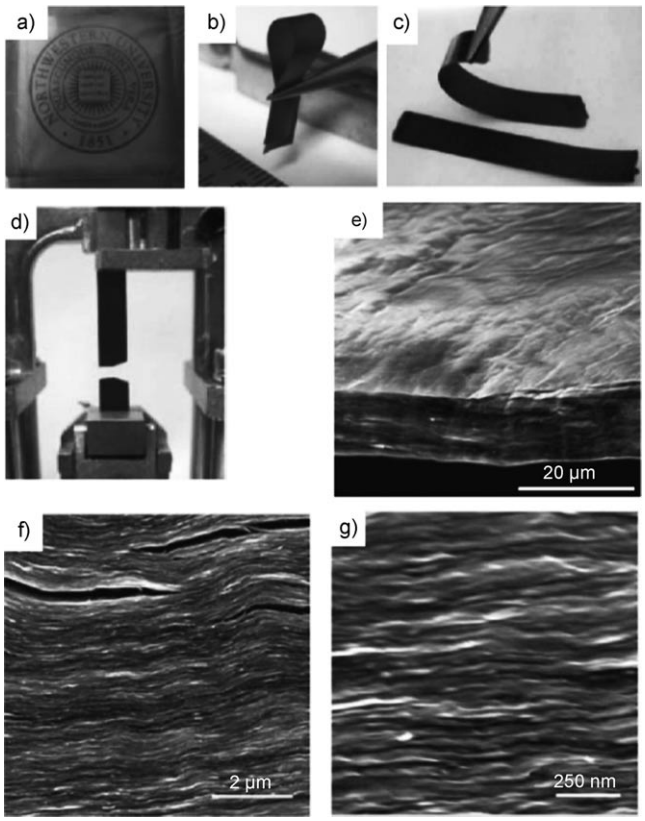

Figure 14. a–d) Digital camera images of graphene oxide paper: a) approximately 1 μm thick; b) folded approximately 5 μm thick semi-transparent film; c) folded approximately 25 μm thick strip; d) strip after fracture from tensile loading. e–g) Low-, middle-, and high-resolution SEM side-view images of an approximately 10 μm thick sample. (From Ref. [52].)

zine and dimethylhydrazine appears to be the promising strategy for the large-scale production of graphene.[55–56] Refluxing graphene oxide in hydrazine or even better, treating graphene oxide with hydrazine in a microwave oven, ensures reduction and produces aggregates of one-to-few (2–3) layer graphenes. Sonication and dispersion in a solvent, such as NMP, favors the formation of a single-layer material. Reduction of graphene oxide with hydrazine is effectively carried out by first coating it with a surfactant, such as sodium dodecylbenzene sulfonate.[55–57] Reaction of the reduced species (coated with the surfactant) with an aryl diazonium salt gives the surfactant-wrapped chemically modified graphene which is readily dispersed in DMF or NMP. Reduced graphene oxide sheets dispersed in organic solvents can also be generated by taking graphite oxide up in an organic phase through the use of an amphiphile, and subsequent reduction with $NaBH_4$.[57]

3. Electronic Structure

The graphene honeycomb lattice is composed of two equivalent carbon sublattices A and B, shown in Figure 15a.

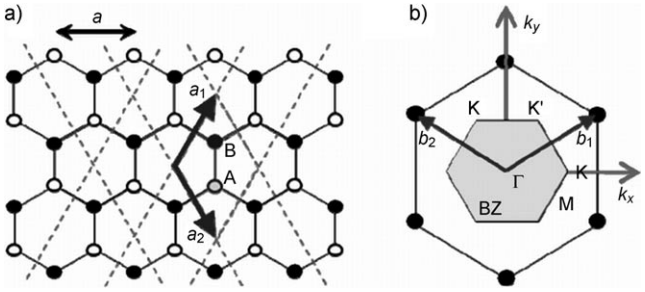

Figure 15. a) Graphene lattice. $\vec{a}_1$ and $\vec{a}_2$ are the unit vectors. b) Reciprocal lattice of graphene. The shaded hexagon is the first Brillouin zone. $\vec{b}_1$ and $\vec{b}_2$ are reciprocal lattice vectors.

Figure 15b shows the first Brillouin zone of graphene, with the high-symmetry points M, K, K′, and Γ marked. Note that K and K′ are the two inequivalent points in the Brillouin zone. The s, p_x and p_y orbitals of carbon atoms form σ bonds with the neighboring carbon atoms. The π electrons in the p_z orbital, one from each carbon, form the bonding π and anti-bonding π* bands of graphene. The dispersion relation of these π electrons is described by the tight-binding model incorporating only the first nearest neighbor interactions [Eq. (1)][58–59]

$$E^{\pm}(k_x, k_y) = \pm\gamma_0\sqrt{1 + 4\cos\frac{\sqrt{3}k_x a}{2}\cos\frac{k_y a}{2} + 4\cos^2\frac{k_y a}{2}} \quad (1)$$

where $a = \sqrt{3}a_{CC}$, a_{CC} is the carbon–carbon distance (1.42 Å), and γ_0, the transfer integral, is the matrix element between the π orbitals of neighboring carbon atoms, its magnitude is approximately 3 eV. The minus sign in Equation (1) refers to the π band which is fully occupied in graphene and the plus sign corresponds to the empty antibonding π^* band. The π and π^* bands touch at the K and K′ points. A Taylor expansion of Equation (1) around K or K′ points yields linear dispersion bands [Eq. (2)].

$$E^{\pm}(k) = \pm\gamma\left|\vec{k}\right| \quad (2)$$

$\vec{k}$ is measured with respect to the K-point, $\gamma = \hbar v_F = \sqrt{3}a\gamma_0/2$, and v_F is the Fermi group velocity. The linear bands, a result of graphene's crystal symmetry, are a hallmark of graphene giving rise to many of the interesting physical properties such as half-integer quantum Hall effect, Berry's phase and Klein paradox.[60,1a,c] Within the linear-band approximation, the constant energy contours are circles around the K and K′ points. The effective Hamiltonian near the K-point can be expressed by the Dirac equation with zero mass [Eq. (3)].

$$H = \begin{pmatrix} 0 & \gamma k \\ \gamma k & 0 \end{pmatrix} = \hbar v_F\,\vec{\sigma}\vec{k} \quad (3)$$

$\vec{\sigma}$ is the 2d pseudospin Pauli matrix. Physically, this implies that the electronic states near the K-point are composed of states belonging to different sublattices A and B and their relative contributions is taken into account using two component wavefunctions (spinors). The eigen functions near K are given by Equation (4)

$$\psi^{o}_{s,k}(\vec{r}) = \frac{1}{\sqrt{2}}\begin{pmatrix} 1 \\ se^{i\theta_k} \end{pmatrix} e^{i\vec{k}.\vec{r}} \quad (4)$$

where $s = \pm 1$ is the band index and $\theta_{\vec{k}}$ is the polar angle of the wavevector $\vec{k}$. Equation (4) reflects that the pseudospin vector is parallel to the wavevector $\vec{k}$ in the upper band ($s = 1$) and is antiparallel in the lower band ($s = -1$). The wavefunctions at K and K′ are related by time-reversal symmetry. The pseudospin and Berry phase may be manipulated by application of an inhomogeneous lattice distortion. Interestingly, a non-constant lattice distortion can lead to a valley-Hall effect, analogous to the spin-Hall effect in semiconductors.[61]

The electronic dispersion of bilayer graphene is different from that of single-layer graphene. The lattice structure of a bilayer graphene is shown in Figure 16a and b. The A_2 sublattice of the top layer is exactly on top of the sublattice B_1 of the bottom layer. In addition to the in-plane nearest-neighbor hopping energy γ_0 (A_1-B_1 or A_2-B_2), there is interlayer hopping energy γ_1 (A_2-B_1). Taking only these two energy scales and neglecting all other hopping energies

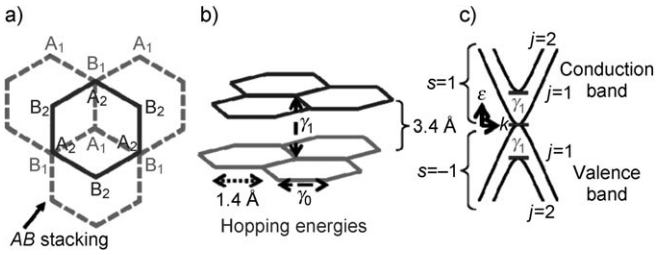

Figure 16. a) Top and b) side view of a bilayer graphene. A_1, B_1 are the sublattices of the bottom layer (broken line) and A_2, B_2 are sublattices of the top layer (solid line). c) Energy dispersion of a bilayer graphene. γ_1 is the energy separation between the two subbands.

(B_2-A_1, A_2-A_1, or B_2-B_1), the Hamiltonian of a bilayer graphene near the K-point can be written as Equation (5).

$$H = \begin{pmatrix} 0 & \gamma k & 0 & 0 \\ \gamma k & 0 & \gamma_1 & 0 \\ 0 & \gamma_1 & 0 & \gamma k \\ 0 & 0 & \gamma k & 0 \end{pmatrix} \quad (5)$$

The eigen values of this Hamiltonian are given by Equation (6)

$$E_{sj}(k) = s\left[\left(\sqrt{\left(\frac{\gamma_1}{2}\right)^2 + (\gamma_0 k)^2}\right)(-1)^j\frac{\gamma_1}{2}\right] \quad (6)$$

where $s = \pm 1$ is a band index, j is a subband index ($j = 1,2$). Figure 16c shows the electronic dispersion of the bilayer, where γ_1 is the energy separation between the two subbands in conduction or valence bands. There is no gap between the valence band and the conduction band. However, a gap can open on application of an electric field perpendicular to the bilayer.[62,63] A band gap has been observed by angle-resolved photoemission experiments on a chemically doped bilayer graphene [64] where the electric field arises through charge transfer from the dopants to the carbon atoms. A direct application of top-gate electric field to the back gated bilayer field effect transistor gives a controlled way to manipulate the band gap, presenting a possibility of electrostatically controlled graphene-based devices.[65]

Quantum Hall Effect: The massless Dirac Fermion nature of carriers in single-layer graphene has interesting consequences on the energy spectrum of the Landau levels (LL) produced in the presence of a magnetic field perpendicular to the graphene layer.[2,3,66] The energies of the Landau levels, indexed by integer j, are given by $E_j = \pm v_F\sqrt{2|j|e\hbar B}$. Notice that E_j is proportional to $\sqrt{B}$, in contrast to conventional two-dimensional electron-gas with parabolic bands where $E_j = \left(j + \frac{1}{2}\right)\hbar eB/m^*$. Furthermore, since the bands touch at the K and K′ points, the $j = 0$ Landau level is shared equally between electrons and holes, whereas in parabolic bands, the first LL is shifted by $\hbar eB/2m^*$. These peculiarities of the Dirac Fermions lead to anomalous quantum hall effect (QHE) with half-integer quantization of the Hall conductivity, instead of an integer quantum hall effect. The Hall

conductivity, σ_{xy}, in single-layer graphene shows a plateau quantized at $\frac{4e^2}{h}\left(j+\frac{1}{2}\right)$ as a function of carrier density, n_s, at a fixed magnetic field or as a function of B at a fixed n_s. Another interesting feature is that the splitting between the LLs ($j=0$ and $j=1$) is 240 meV at 45 T which makes the observation of quantum hall effect possible at room temperature.[4]

For bilayer graphene, the quasi-particles are chiral but with a finite mass. The Landau levels in this case are given by $E_j=\pm\frac{\hbar eB}{m^*}\sqrt{j(j-1)}$, leading to two degenerate levels $j=0$ and $j=1$ at zero energy. This situation results in the absence of the zero-energy plateau, $\sigma_{xy}=j4e^2/h$, where j is an integer except $j=0$.[67] The opening of a gap in bilayer graphene by the electric field is also reflected in the quantum hall plateaus.[68]

4. Phonons and Raman Spectroscopy

Single-layer graphene belongs to the D_{6h} point group which reduces to D_{3d} for the AB bilayer and ABC trilayer, and to D_{3h} for the ABA trilayer. The zero-wavevector ($q=0$) optical phonons in single-layer graphene belong to the irreducible representations $E_{2g}(R)$ and $B_{2g}(IR)$, where R and IR refer to Raman and infrared active modes. The eigen vectors of these optical modes (Figure 17a) show that the E_{2g} mode (degenerate transverse optic (TO) and longitudinal optic (LO)) is an in-plane optical vibration with the frequency 1582 cm^{-1}.[69,70] The two neighboring atoms vibrate opposite to one another, resulting in large bond distortions. In the B_{2g} mode, the carbon atoms move perpendicular to the graphene plane. For bilayer graphene with AB stacking with four atoms per unit cell, the optical modes are $2E_g(R)$, $2E_{1u}(IR)$, $A_{2u}(IR)$, $2B_{1g}$. The eigen-vectors of E_g and E_{1u} are shown in Figure 17b. The IR active E_{1u} mode is slightly higher in frequency (ca. 7 cm^{-1}) than the Raman E_g mode.

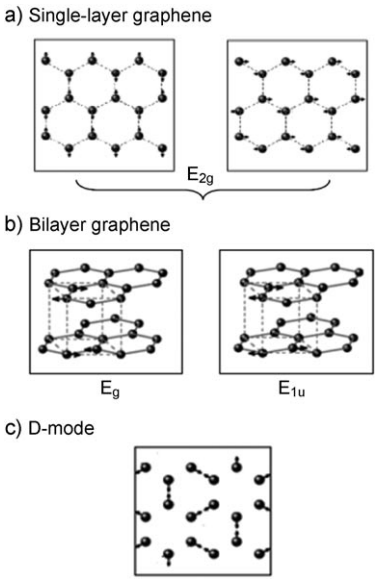

Figure 17. a) Atomic displacements for the E_{2g} (TO/LO) modes at Γ in single-layer graphene. b) Atomic displacements of $E_g(R)$ and $E_{1u}(IR)$ modes at Γ for bilayer graphene. One mode for each degenerate pair is shown. c) Atomic displacements for the highest TO mode at K. (From Ref. [70].)

Vibrational properties of ultrathin n-layer graphene ($n=$ 1–7) have been studied using first-principal density functional (DFT) theory.[71] It is found that a low-frequency optical phonon (ca. 110 cm^{-1}) with out-of-plane displacements exhibits a large sensitivity to the number of layers, although the interlayer spacing does not change appreciably as n varies. This low-frequency mode is yet to be observed experimentally but could prove to be a marker for the number of layers.

Figure 18 shows the phonon dispersion of single-layer graphene using DFT.[70] The branch indexed as ZA refers to the out-of-plane acoustic mode which has a q^2 dispersion, in

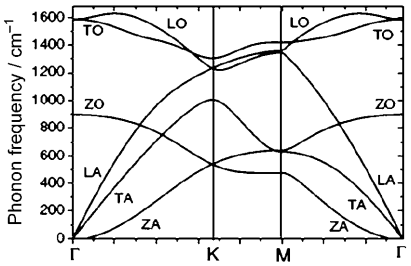

Figure 18. Phonon dispersion for monolayer graphene. (From Ref. [70].)

contrast to the linear q dispersion of the longitudinal and transverse acoustic modes. Many recent calculations have discussed the important issue of electron–phonon coupling in graphene.[72–77] The degenerate E_{2g} phonon at Γ and the highest TO phonon at K have strong electron–phonon interactions, resulting in Kohn anomalies in the phonon dispersion. The Kohn anomaly refers to the anomalous screening of phonons of wavevector $\mathbf{q}$ which can connect two points $\mathbf{k_1}$ and $\mathbf{k_2}$ on the Fermi surface such that $\mathbf{k_2}=\mathbf{k_1}+\mathbf{q}$.[78] For graphene and metallic nanotubes, the Kohn anomalies occur at $\mathbf{q}=\mathbf{0}$ and $\mathbf{q}=\mathbf{K}$. The eigen vectors of the phonon modes responsible for the Raman D-band transform according to the A_1 and B_1 representations of C_{6v} and are shown in Figure 17c.[70,79] The two sublattice atoms move circularly in opposite directions.

Raman spectroscopy is a powerful probe for characterizing sp^2 and sp^3 hybridized carbon atoms—be they in graphite, diamond-like carbon, diamond, polyaromatic compounds, fullerenes, or carbon nanotubes. Raman fingerprints of single, bi-, and few-layer graphenes are different and have been investigated by several groups.[13,14,16,80–83] A typical Raman spectrum of single-layer graphene is shown in Figure 19. The symmetry allowed E_{2g} mode at the Γ-point, usually termed as the G-mode, appears at approximately 1583 cm^{-1}. The other Raman modes seen are at 1350 cm^{-1}(D-mode), 1620 cm^{-1}(D′-mode), 2680 (2D- or D*-mode), 2950 (D + G-mode), 3245-(2D′-mode) and 4290 cm^{-1}(2D+G-mode). The D-mode, is a disorder-activated Raman mode and is associated with the TO branch near the K-point. Its frequency depends on the incident laser energy (ca. 50 cm^{-1} eV) and has been under-

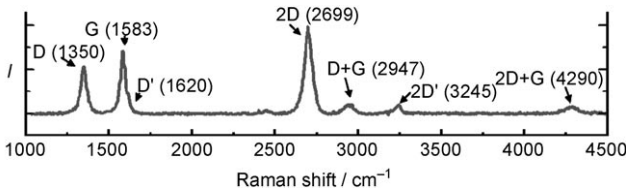

Figure 19. Typical Raman spectrum of single-layer graphene prepared by mechanical exfoliation. The excitation laser wavelength was 514.5 nm.

stood[84–86,69] based on the double-resonance Raman process shown in Figure 20. The Raman tensor can be written in fourth-order perturbation theory as Equation (7).

$$R = \sum_{a,b,c} \frac{M_{er} M_{e-def} M_{ep} M_{er}}{(E - E_a - i\gamma)(E - \hbar\omega_p^q - E_b - i\gamma)(E - \hbar\omega_p^q - E_c - i\gamma)} \qquad (7)$$

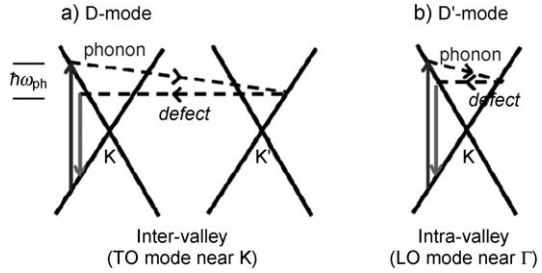

Figure 20. a) and b): Double-resonance Raman scheme for the D- and D′-modes. Vertical solid lines represent interband electronic transitions accompanied by photon absorption or emission. Dashed arrow represents phonon emission and horizontal dashed line represents the defect scattering.

E_L is the energy of the incident laser photon, M the matrix elements, and γ is the life-time broadening of the intermediate electronic states a, b, and c. Figure 20a shows the four steps involved in defect-assisted Raman process: 1) electron–radiation interaction with matrix element M_{er}, 2) electron–phonon interaction (M_{ep}) making a phonon assisted inter-valley transition, 3) defect-assisted transition M_{e-def} to take care of the momentum conservation, and 4) the electron–radiation interaction. In the double-resonance Raman process, the phonon with wavevector **q** is so chosen that the energy denominator is minimum. A change in the incident photon energy results in a phonon of different wavevector on the TO branch being chosen and hence the shift in the D-mode frequency arises through the dispersion of the phonon branch near the K-point of the Brillouin zone. The mode at 1620 cm^{-1}, termed as D′, also arises through the double-resonance process, as a result of intra-valley scattering involving the LO phonon near the Γ-point (Figure 20b).

The mode at 2680 cm^{-1} is the second-order Raman scattering involving TO phonons near the K-point. It is labeled as the D*- or 2D-mode. Unlike the D-band, disorder is not required for the wavevector conservation because two-phonons of equal and opposite momentum can satisfy the Raman requirement of $q \approx 0$. Hence, the 2D band can be observed in the Raman spectra, even though the D-mode is absent (see Figure 22). Like the D-band, this Raman band is highly dispersive with changing incident photon energy (ca. 100 $cm^{-1}\,eV^{-1}$), almost twice of the dispersion of the D-band. Double resonance Raman scattering shown in Figure 21a can

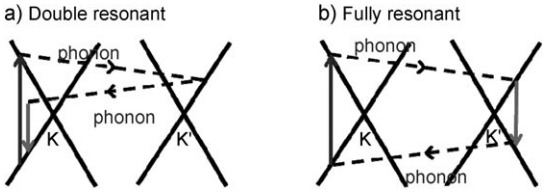

Figure 21. Double-resonance Raman process for the two-phonon Raman scattering. Notation same as in Figure 20.

quantitatively explain the dependence of the 2D Raman band frequency on the laser photon energy. It has been pointed out[87] that the Raman process shown in Figure 21b, labeled fully resonant, is more dominant than the double resonance process. In bilayer graphene, the electronic dispersion is different from that in single-layer graphene (See Figure 16c) and hence the shape of 2D band is different from that in single-layer graphene.[14,16] Figure 22 shows the comparative Raman spectra of mono- and bi-layer graphenes along with the spectrum of HOPG. Ferrari et al.[14] have shown that the 2D band in bilayer graphene can be decomposed into four bands arising from the different phonon-assisted inter-valley transitions shown in Figure 23. It is found[80] that the position of the Raman G-band in mechanically exfoliated single-layer graphene varies from 1582 cm^{-1} to 1594 cm^{-1}. The line-width also varies from 20 cm^{-1} to 14 cm^{-1}. Figure 24 shows the variation of the G-mode frequency ω_G and its full-width-at-half-maximum (FWHM) as a function of the intensity ratio of the D- and G-modes, $I(D)/I(G)$. The ratio is a measure of the disorder in the sample, which can be edges, charge puddles, ripples, or any other defects. The data in Figure 24 reflect the unintentional charge doping of the graphene by defects (see below). The intensity of D-band is related to the edge chirality.[88] It is weak at the zigzag edge and strong at the armchair edge.

Raman spectra are routinely used to characterize graphene samples. Raman spectra of few-layer graphenes prepared by different methods are shown in Figure 25.[1c] The shift and splitting of Raman modes can be used to determine the strain in graphene layers. Raman spectra of epitaxial graphene layers grown on SiC show a significant blue shift of the G-band (ca. 20 cm^{-1}) and 2D bands (ca. 60 cm^{-1}) compared to exfoliated graphene.[89–91] This shift mainly arises due to compressive strain that builds up when sample is cooled down after annealing.

In graphene monolayer under uniaxial strain, the doubly degenerate E_{2g} mode splits into two components—one polarized along the strain and the other perpendicular to it.[92–95] This results in splitting of the G-band into two bands G^+ and G^- which are red shifted under the uniaxial tensile strain. The red shifts for 1% strain are 11 cm^{-1} for G^+ band

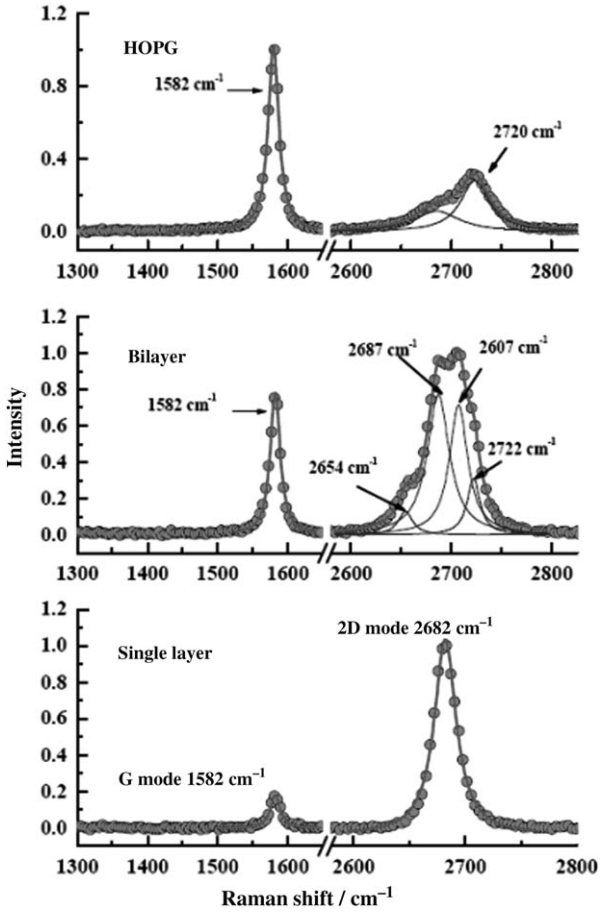

Figure 22. Raman spectra of single-layer graphene and bilayer graphene prepared by mechanical exfoliation of HOPG. Note that even though the D-mode is absent in graphene samples, the 2D-mode is strong. The 2D band in bilayer graphene is deconvoluted into four bands arising from the double resonance processes. (From Ref. [80].)

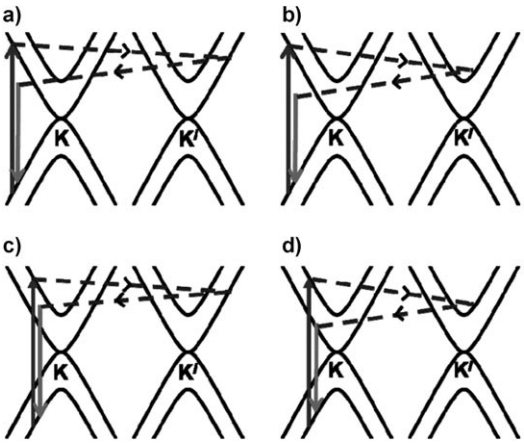

Figure 23. Schematic representation of all the four possibilities in a double-resonance Raman process. The solid vertical lines are electronic transitions and the dashed lines represent emission of phonons.

and 32 cm^{-1} for G^- band.[92] For the 2D band, the corresponding shift is 64 cm^{-1}, which can also have contributions from the changes in the phonon wavevector arising from

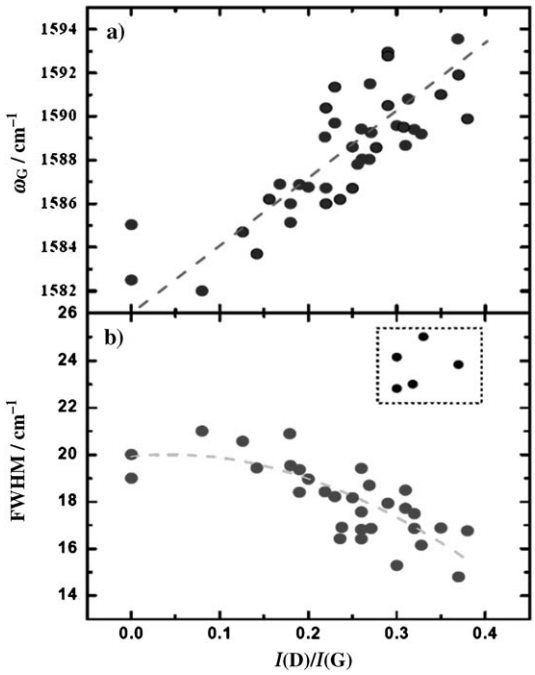

Figure 24. Peak position of the G-mode, ω_G, and its FWHM of single-layer graphenes as a function of the $I(D)/I(G)$ ratio. The dashed lines are a guide for the eye. (From Ref. [80].)

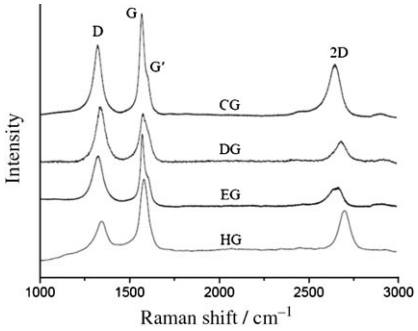

Figure 25. Raman spectra of a) CG, b) DG, c) EG, and d) HG. (From Ref. [1d].)

relative movement of the Dirac cones.[92] This effect can contribute to the asymmetric broadening of the 2D band.

5. Effects of Doping

5.1. Electrochemical Doping

Doping of graphene is easily achieved by using the commonly used SiO_2 back-gated field effect transistor (FET) geometry. In situ Raman measurements on such devices[96–97] reveal that the frequency of the G-band increases whereas the line-width decreases for both electron and hole doping. The doping level achieved is 5×10^{12} cm^2. A novel method to achieve an order-of-magnitude higher doping is to use electrochemical top gating, where the Debye layer of thickness of approximately 1 nm acts as a gate, with a much higher

gate capacitance C_G.[98] Recall C_G is proportional to $1/d$ where d is the thickness of the gate layer and is typically around 300 nm for SiO_2 back-gated field effect transistor. The electrochemical top gating results in $C_G \approx 2 \times 10^{-2}\,F\,m^{-2}$, about 170 times higher than the SiO_2 back-gated field effect transistor. Figure 26a is a schematic diagram of the experimental set up[99] to monitor the effect of doping on Raman modes using top gating with a solid ($LiClO_4$)/polymer (polyethylene oxide; PEO) electrolyte. Figure 26b shows the transistor characteristics of the top-gated field effect transistor. The dependence of the peak position, Pos(G), and the full-width-at-half-maximum, FWHM(G) of the G-band, as well as of the position of the 2D band, Pos(2D), on electron and hole concentrations are shown in Figure 27. We see that the Fermi level can be shifted by as much as 0.7 eV with top gating. The important points to note from Figure 27 are: 1) Pos(G) increases for both electron and hole doping 2) the FWHM(G) decreases on doping and becomes independent of doping when Fermi energy shift is larger than half the phonon energy ($\hbar\omega_G/2$), 3) the doping dependence of the 2D band is very different from that of the G-band. The 2D band wavenumber increases for hole doping and decreases for electron doping, thereby establishing that the amount and nature of doping can be determined simply by studying both the G and 2D bands. Another important result that has come out of this study is that the intensity ratio of 2D and G bands, I(2D)/I(G) depends on the doping (Figure 28). Therefore, if the graphene sample is unintentionally doped, as is usually the case, I(2D)/I(G) and Pos(G) should not be used to estimate the number of layers. The solid lines in Figure 27 represent the results from theoretical calculations (see below).

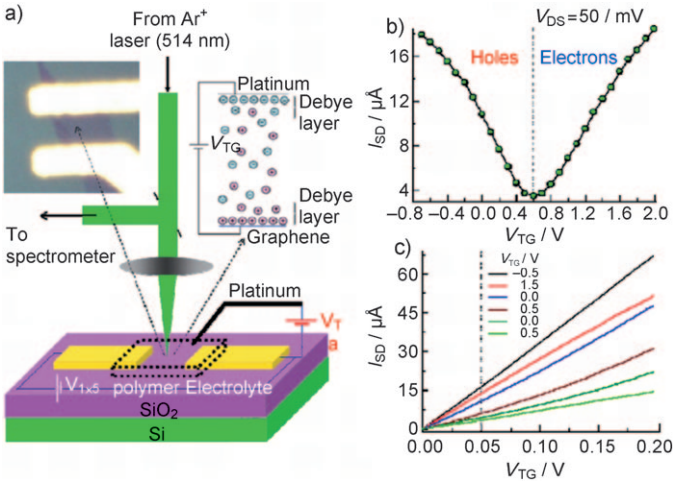

Figure 26. a) Schematic representation of the experimental set up for using top gating to study the influence of doping on the Raman modes. The left inset shows the optical image of a single-layer graphene connected between source and drain gold electrodes. The right inset is a schematic illustration of polymer electrolyte top gating. b) Source-drain current I_S as a function of top-gate voltage V_{TG} at a fixed source-drain voltage V_{DS}. c) I_{SD} versus V_{DS} for different V_{TG} values. (From Ref. [99].)

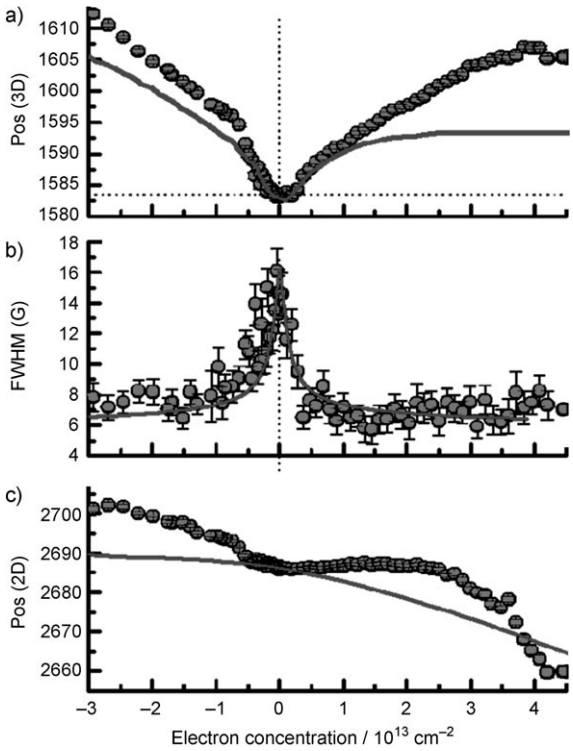

Figure 27. Doping dependence of a) the position Pos(G) and b) line width FWHM(G) of the G-mode, and c) the postion Pos(2D) of the 2D-mode. The solid lines are theoretical curves. (From Ref. [99].)

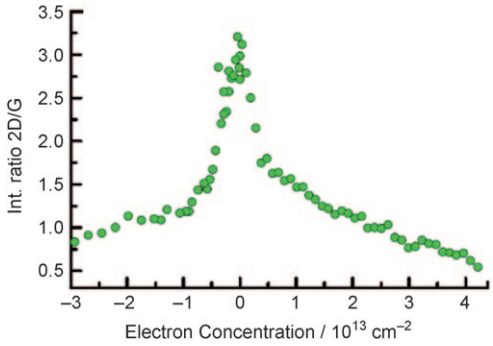

Figure 28. Dependence of the I(2D)/I(G) on doping. (From Ref. [99].)

Doping has two major effects: 1) a change in the equilibrium lattice parameter (electron doping results in expansion of the lattice giving rise to phonon softening whereas hole doping results in contraction of the lattice giving rise to phonon stiffening) and 2) effects beyond the adiabatic Born–Oppenheimer (ABO) approximation which alter the phonon dispersion close to the Kohn anomalies (KA).[75,96–97,100] The reason for going beyond the often used ABO approximation is that the electron-momentum relaxation time in graphene is much larger than the phonon pulsation time (ca. 3 fs) and hence the phonon is a dynamic perturbation to the electronic system. For the 2D band, however, dynamic effects are expected to be small, since the phonons giving rise to the 2D band are far away from the Kohn anomaly at K-point.[101] Physically, G-peak stiffening is

due to the non-adiabatic removal of the Kohn anomaly at Γ. The reduction in FWHM(G) is due to the blockage of phonon decay into an electron–hole pair when the electron–hole gap is higher than the phonon energy, which saturates for a Fermi shift larger than half-phonon energy. We see from Figure 27 that agreement between theory and experiment for both the G- and 2D-bands is modest and hence a complete understanding of phonon renormalization is yet to emerge. A possible means to improve the agreement can be to include electron–electron correlations which can be important as doping increases.

Since the electronic structure of bilayer graphene is different from single-layer graphene, the phonon response to doping will be different.[111] Recently, the effects of doping on the phonons in bilayer graphene have been studied.[103–104] Recall that the bilayer has two conduction bands and two valence bands, the splitting of which depends on the interlayer transfer integral γ_1. Raman measurements of the change in the G-band frequency with doping has allowed a direct measurement of γ_1.[105] Figure 29a shows the Raman spectra

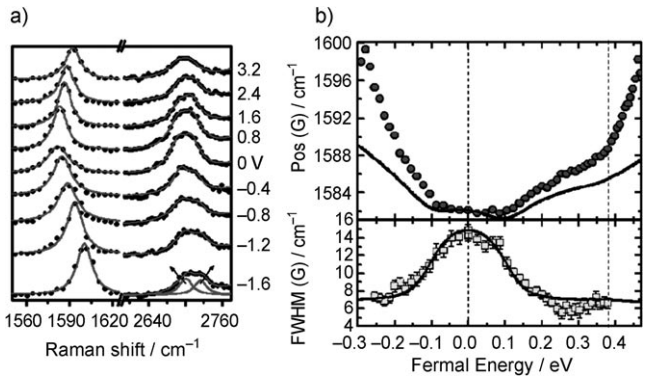

Figure 29. a) Raman spectra of a bilayer graphene at various gate voltages. b) Pos(G) and FWHM(G) as a function of Fermi energy shift. Fermi energy is tuned by electrochemical top gating using solid polymer electrolyte. Solid lines are theoretical predictions incorporating dynamic effects beyond the adiabatic Born-Oppenheimer approximation. (From Ref. [105].)

of a bilayer graphene at a few values of top-gate voltages. The filled circles in Figure 29b show Pos(G) and FWHM(G) of bilayer graphene as a function of Fermi-energy shift.[105] The solid lines are from theoretical calculations taking into account the change in lattice parameter as well as dynamic contributions calculated using time-dependent perturbation theory.[105] The main features of the phonon renormalization in bilayer graphene are as follows: Like single-layer graphene, Pos(G) does not increase up to $E_F \approx 0.1$ eV (ca. half of the phonon energy). The FWHM(G) decreases for both electron and hole doping. With a Fermi energy shift of 0.1–0.4 eV, the slope d[Pos(G)]/d(E_F) is smaller in bilayer graphene than in single-layer graphene. A significant result is the observation of a kink in Pos(G) at $E_F \approx 0.4$ eV, corresponding to the γ_1 value. Das et al.[105] have quantitatively explained that the kink arises from the filling of the second subband which blocks some intraband transitions.

5.2. Doping by Molecular Charge Transfer

Interaction of graphene with electron-donor and electron-acceptor molecules causes marked changes in the electronic structure and properties of graphene.[106,107] Thus, electron-donor molecules, such as aniline and tetrathiafulvalene (TTF), soften (i.e. shift to lower frequency) the Raman G band of few-layer graphene while electron-acceptor molecules, such as nitrobenzene and tetracyanoethylene (TCNE), stiffen (i.e. shift to higher frequency) the G band. In Figure 30

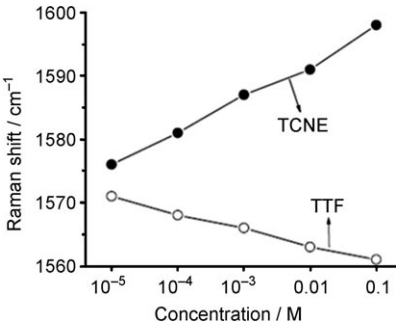

Figure 30. Variation of the G-band frequency with the concentration of electron-donor (TTF) and electron-acceptor (TCNE) molecules. (From Ref. [107].)

we show the variation of the G-band frequency with the concentration of electron-donor (TTF) and -acceptor (TCNE) molecules. The width of the G band increases on interaction with these molecules. The width of the D band also varies on interaction with electron-donor and electron-acceptor molecules. The intensity of the 2D band decreases markedly on interaction with electron-donor and electron-acceptor molecules (Figure 31a). The ratio of intensities of the 2D and G bands, I(2D)/I(G), is a sensitive probe to examine the effect of the electron-donor and electron-acceptor molecules on the electronic structure of graphene. In Figure 31b, we show how the I(2D)/I(G) ratio decreases markedly with the concentration of both TTF and TCNE. The I(D)/I(G) intensity ratio shows an opposite trend. This is because the origins of D and 2D Raman bands are different. Charge-transfer bands are found in the visible region when TTF and TCNE interact with few-layer graphene (Figure 32). DFT calculations confirm the occurrence of charge-transfer-induced changes in graphene and show how they are different from the effects of electrochemical doping.[108] The effects of donor and acceptor molecules discussed above also occur with single-layer graphene.

Electrical conductivity of graphene also varies on interaction with both electron-donor and electron-acceptor molecules. Electron-donor molecules decrease the conductivity of graphene while electron-acceptor molecules increase the conductivity. The magnitude of interaction between the different graphenes and donor/acceptor molecules is found to be dependent on surface area of the graphene samples.[109]

Adsorption of H_2O, NH_3, CO, NO_2, and NO on graphene involves charge-transfer between the molecules and the graphene surface[110,111] The magnetic moment of molecules

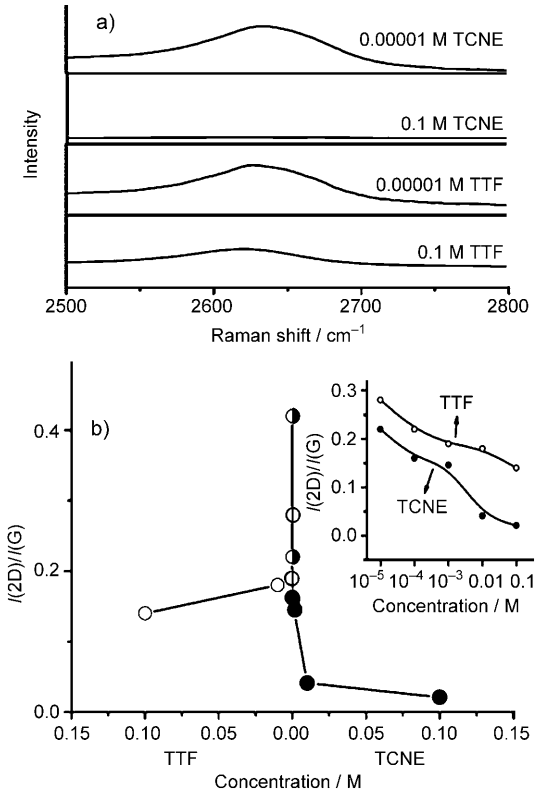

Figure 31. Variation in a) the Raman 2D-bands and b) the $I(2D)/I(G)$ ratio of graphene with the concentration of TTF and TCNE. Inset in (b) shows the plots of $I(2D)/I(G)$ against the logarithm of the concentration. (From Ref. [107].)

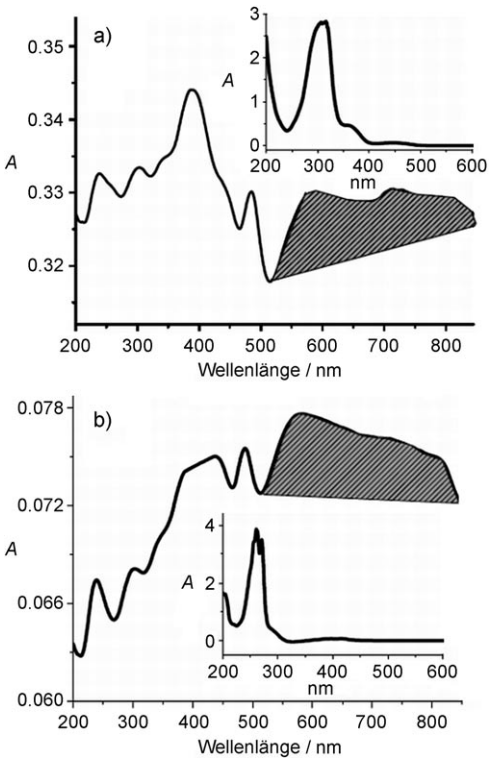

Figure 32. Electronic absorption spectra of a) graphene + TTF and b) graphene + TCNE. Inset in (a) the spectra of TTF and in (b) the spectra of TCNE. The shaded regions correspond to the charge-transfer bands. (From Ref. [107].)

also seems to influence the doping efficiency. It has been shown that two different types of charge-transfer mechanisms operate, one arising from orbital hybridization and the other is due to the position of HOMO and LUMO of the molecule with respect to the Dirac-point of graphene.[111] As well as calculation of the adsorption energies, the optimal adsorption position and orientation of the molecules on the graphene surface was also determined.[110] Depending on the level of doping it can be determined whether the adsorbate is a closed or open shell system. The open-shell NO_2 molecule is found to be a strong acceptor, whereas its closed-shell counterpart N_2O_4 causes only weak doping.[112]

5.3. Doping by Substitution with Boron and Nitrogen

B-doped and N-doped bilayer graphene samples have been prepared recently by employing different strategies and their structure and properties investigated.[113] B-doped graphene have been prepared by two methods involving arc discharge of graphite electrodes in the presence H_2 and B_2H_6 and by carrying out arc discharge using a boron-filled graphite electrodes (3 atom% boron). Nitrogen-doped graphene has been prepared by carrying out arc discharge in the presence of H_2 and pyridine or H_2 and ammonia. Transformation of nanodiamond in the presence of pyridine also yields N-doped graphene. The Raman G band is found to move to higher frequency both with boron and nitrogen doping in comparison with the undoped sample. This situation is similar to what happens with electrochemical doping.[92,99] The intensity of the D band is higher with respect to that of the G band in all the doped samples. On doping, the relative intensity of the 2D band generally decreases with respect to the G band. DFT calculations have been carried out to understand the effect of substitutional doping on the structure of graphene as well as its electronic and vibrational properties.[113]

6. Functionalization and Solubilization

Carbon nanotubes (CNTs) have been functionalized by both covalent and noncovalent means to disperse or solubilize them in different solvents.[114,115] Functionalization of graphene has been carried out by employing similar strategies.[1d] For example, Haddon and co-workers have functionalized graphene with covalently bound groups. Acid-treated graphene containing surface OH and COOH groups was first allowed to react with $SOCl_2$ to create COCl groups, subsequent reaction with a long-chain aliphatic amine gave the amide derivative which is soluble in nonpolar solvents.[116a] Another method employed by these workers is grafting aryl groups through diazotization reactions.[116b] Soluble graphene layers in THF can be generated by the covalent attachment of alkyl chains to graphene layers by the reduction of graphite fluoride with alkyl lithium reagents.[116c] Such covalent

functionalization enables solubilization in organic solvents, such as CCl_4, CH_2Cl_2, and THF (Figure 33a).[47] Similar procedures have also been employed by Subrahmanyam et al.[1d,117] Figure 33a shows photographs of dispersions of few-layer graphene in nonpolar solvents. The reaction of graphene with a mixture of concentrated H_2SO_4 and HNO_3 gives water-soluble graphene which is stable for several months (see Figure 33b). Graphene is solubilized in CCl_4 by interaction with organosilane and organotin reagents, such as hexadecyltrimethoxysilane (HDTMS) and dibutyldimethoxytin (DBDT), as can be seen from Figure 33c and d, respectively.[117]

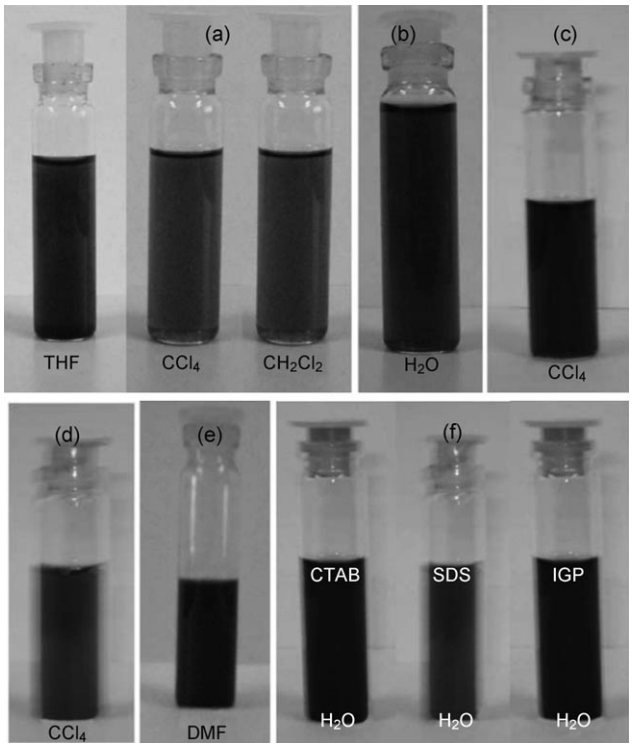

Figure 33. Photographs of a) dispersions of the amide-functionalized EG in THF, CCl_4, and dichloromethane, b) water soluble EG, c) dispersion of HDTMS-treated EG in CCl_4, d) dispersion of DBDT-treated EG in CCl_4, e) dispersion of PYBS-treated EG in DMF and f) water dispersions of EG treated with CTAB, SDS, and IGP. (From Ref. [47,117].)

Graphene can be functionalized through noncovalent modification without affecting its electronic structure by wrapping with surfactants or through π–π interaction with a pyrene derivative such as 1-pyrenebutanoic acid succinimidyl ester (PYBS).[117] Through the π–π interaction with PYBS, graphene becomes soluble in DMF (Figure 33e). Noncovalent interaction of graphene with surfactants, such as Igepal CO-890 (polyoxyethylene(40)nonylphenylether; IGP), sodium dodecylsulfate (SDS), and cetyltrimethylammonium-bromide (CTAB) gives water-soluble graphene (Figure 33f).[117] Water-soluble graphene can also be prepared by the PEGylation method in which, acidified graphene is treated with excess of polyethylene glycol (PEG) and conc. HCl under solvothermal conditions.[47,118]

Chemically converted graphene sheets obtained from the reduction of surfactant-wrapped graphene oxide with hydrazine have been functionalized by treatment with aryldiazonium salts.[119] The resulting graphene sheets are dispersible in polar aprotic solvents, such as DMF (Figure 34). Aqueous dispersions of graphene have been obtained by carrying out the reduction of graphene oxide with hydrazine hydrate in the presence of poly(sodium-4-styrenesulfonate) or KOH.[56,120b] Sonication of 7,7,8,8-tetracyanoquinodimethane (TCNQ)-treated expanded graphite, followed by centrifugation[120c] and reduction of the resulting sulfonated graphene oxide with hydrazine,[129d] yields water-soluble graphene. TCNQ-anion stabilized graphene is also soluble in DMF and dimethyl sulfoxide (DMSO; Figure 35). Basal-plane hydrogenation of graphene has been carried out by using hydrogen atoms generated in situ by electron-induced dissociation of hydrogen silsesquioxane.[121] Hydrogenation proceeds at a higher rate for single-layer graphene than bilayer graphene demonstrating the enhanced chemical reactivity of single-layer graphene. This enhance reactivity was also indicated by Raman spectroscopy (Figure 36). Functionalized graphite platelets comprising 6 to 23 graphene sheets have been prepared by the reductive alkylation of fluorinated graphite. The functionalized platelets are soluble in $CHCl_3$, CH_2Cl_2, DMF, DMSO, and benzene.[122] Exfoliation of isocyanate-treated graphite oxide gives functionalized graphene oxide platelets, which are soluble in polar aprotic solvents.[123] Chemical modification of graphene has been accomplished by several other means which include functionalization with a porphyrin,[124a] with an ionic liquid,[124b] and electrochemically. Dodecylated nanographite which is soluble in nonpolar

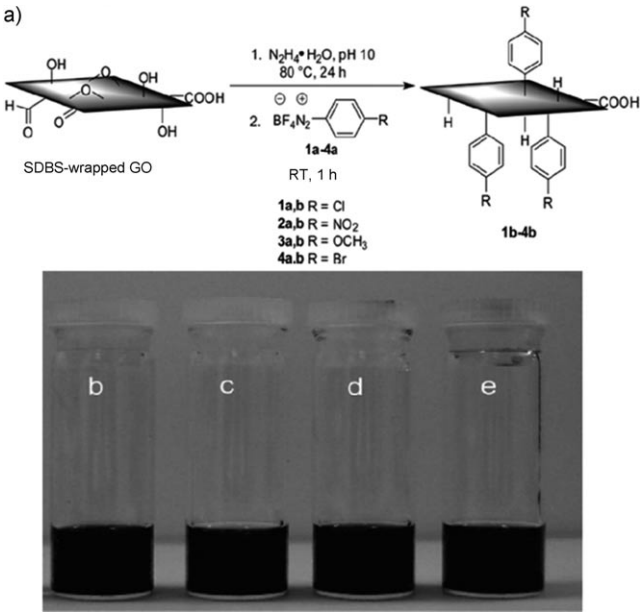

Figure 34. a) Reduction of SDBS-wrapped graphite oxide and functionalization of the intermediate, SDBS-wrapped chemically modifide graphene (CCG), with diazonium salts. Photographs of supernatant DMF solutions obtained from b) **4b**, c) **1b**, d) **2b**, and e) **3b** after centrifugation for 15 min at 3200 rpm. (From Ref. [119].)

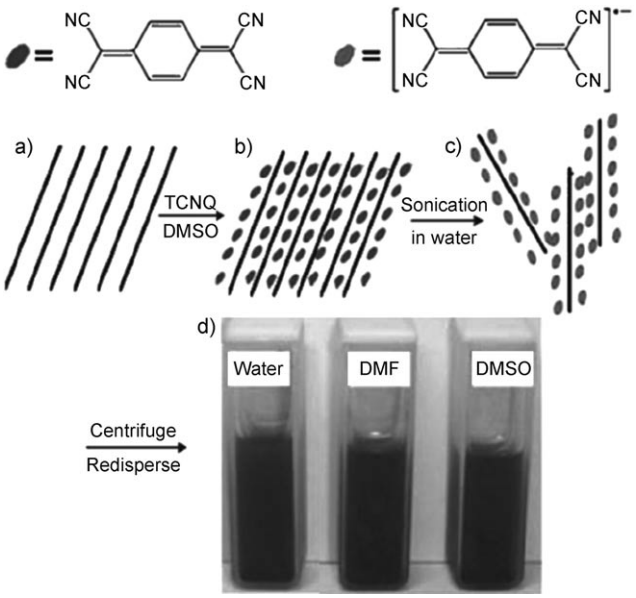

Figure 35. Aqueous graphene dispersions stabilized with TCNQ anion. a) Expanded graphite. b) TCNQ-intercalated expanded graphite (with the aid of DMSO). c) TCNQ-anion-stabilized graphene in water by sonication. d) Photograph of TCNQ anion adsorbed graphene dispersed in water, DMF, DMSO. (From Ref. [120b].)

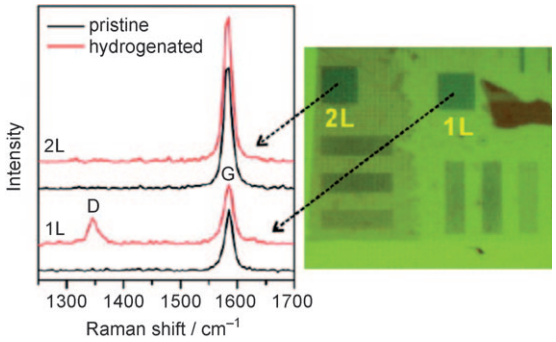

Figure 36. Optical micrograph of electron-beam patterned graphene containing single (1L) and bilayers (2L) and the corresponding Raman spectra before (pristine) and after hydrogenation. (From Ref. [121].)

solvents has been obtained starting from potassium graphite[124d]. Molecular dynamics simulation studies show that pristine graphene sheets agglomerate in nonpolar media whereas graphene sheets functionalized at the edges with short branched alkanes yield stable dispersions.[125]

Controlled cutting of graphene sheets, using nickel nanoparticles as a "knife" has been described.[126] The cutting proceeds by catalytic hydrogenation of the graphene lattice, and can generate graphene pieces with specific zigzag or armchair edges (Figure 37).

7. Decoration with Metal and Metal Oxide Nanoparticles

Carbon nanotubes decorated with metal nanoparticles are expected to be useful in catalysis, nanoelectronics, optics, and

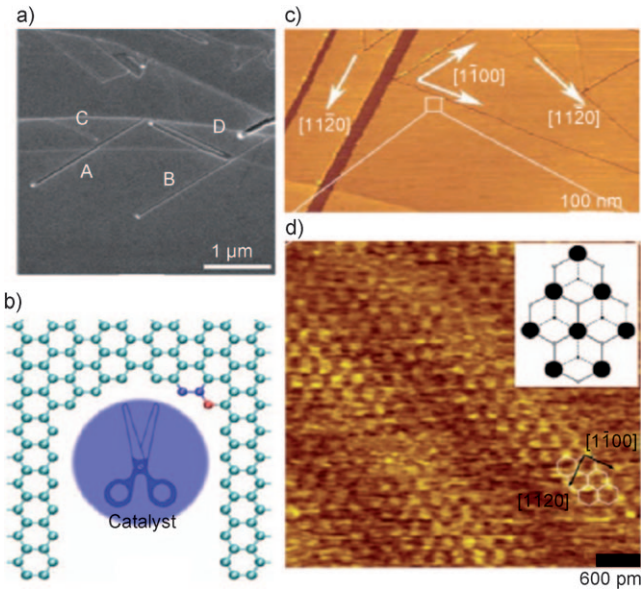

Figure 37. a) Nanocutting of graphene by SEM. The cutting starts at step sites and the nanoparticles end up at the end of the cut channels. b) Monte Carlo simulations of the formation of a zigzag-edged channel. c) STM images of nano-channels in different directions. d) Magnified image with atomic resolution showing the crystallographic orientation of graphene. Inset: graphite crystal structure. (From Ref. [126].)

nanobiotechnology.[114] Graphene can be decorated with nanoparticles of metals such as Au and Pt.[127] Decoration can be carried out in a single step by the polyol reduction method using chloroplatinic acid, silver nitrate, or chloroauric acid as the metal precursors.[1d,128] On coating with the metal particles, the intensity of the Raman D band increases while that of the 2D band decreases, which is an effect of Columbic charge transfer from the metal nanoparticles. Graphene has also been decorated with Au, Pt, and Pd nanoparticles in a water/ethylene glycol system using graphene oxide as the precursor.[129] Metal nanoparticles adsorbed on graphene oxide sheets, play a role in the catalytic reduction of graphene oxide with ethylene glycol. Copper nanoparticles have been coated with protective shells of graphene by employing reductive flame synthesis.[130] Graphene-coated copper nanoparticles can be used as air-stable substitutes for silver and gold in low-cost ink-jet-printable electronics. Platinum nanoparticles deposited on graphene can be used to prevent the aggregation of sheets during the reduction of graphene oxide.[131]

Few-layer graphenes can be etched along crystallographic axes by thermally activated metallic nanoparticles, a process that can be useful for construction of integrated circuits.[132]

Ultrathin layers of Al_2O_3 can be uniformly deposited on graphene that is noncovalently functionalized with carboxylate-terminated pyrene molecules (Figure 38).[133] Co_3O_4 nanoparticles have been deposited on exfoliated graphite oxide sheets by stirring a mixture of exfoliated graphite oxide and cobalt nitrate hexahydrate in *n*-hexanol and then heating.[134a] TiO_2-graphene nanocomposites are obtained by photocatalytic reduction of graphite oxide.[134b]

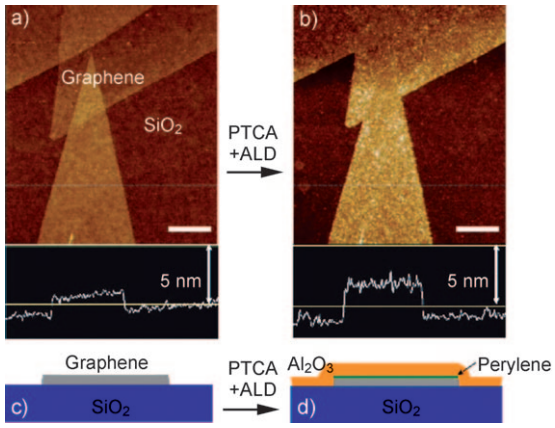

Figure 38. AFM images of graphene on SiO_2 a) before and b) after atomic layer deposition (ALD) of Al_2O_3. The height profile shows the thickness of the triangular shaped graphene is approximately 1.6 nm before deposition and approximately 3 nm after deposition. c),d) Schematic representations of graphene on SiO_2 c) before and d) after ALD. Scale bar: 500 nm. (From Ref. [133].) PTCA = 3,4,9,10-perylene tetracarboxylic acid.

8. Properties

8.1. Magnetic Properties

Magnetism in carbon-based materials with networks of sp^2 hybridized carbon atoms has been controversial because of possible contamination with magnetic impurities. It has been noted, however, that edges in graphene ribbons play a crucial role in determining the electronic structure,[135] the zigzag edges with nonbonding-electrons giving rise to the edge states. The structure and electronic properties of nanographite particles and ribbons have been studied by a few workers to demonstrate the importance of edge states.[49,136–137] Paramagnetism as well as certain other magnetic features including spin-glass behavior and magnetic switching phenomena have been observed in nanographite particles.[49,136–137] Hydrogenated nanographite is predicted to show spontaneous magnetism.[138] Magnetic properties of nanographite or nanographene have been reviewed by Enoki et al.[139–141] and the main message is that the edge states as well as of adsorbed or intercalated species play an important role in determining the magnetic properties. Adsorption of different guest molecules on graphene gives rise to a reversible low-spin/high-spin magnetic-switching phenomenon which depends on the nature of the guest species. Enoki et al. suggest that the unusual properties of nanographite may be tailored by cutting in certain directions. Theoretical studies have shown the existence of a ferromagnetically ordered ground state in the zigzag edges and also the importance of the crystallographic nature and of the possible half-metallicity of graphene.[142] Zigzag edges longer than three to four repeat units are predicted to be magnetic irrespective of whether the edges are regular or irregular.[143a] Stacking faults and other defects can also impart ferromagnetism and antiferromagnetic features in graphene.[143b] According to a geometric rule for nanomagnetism, parallel spins give rise to ferromagnetism whereas antiparallel spins cause antiferromagnetism.[144] Room-temperature ferromagnetism has been reported recently in graphene and it is believed to come from defects.[145] Enoki et al.[146] have demonstrated how the magnetoresistance of nanographite is significantly affected by adsorption of oxygen.

Magnetic properties of the few-layer graphenes EG (prepared by exfoliation of graphite oxide), DG (prepared by the conversion of nanodiamond), and HG (prepared by the arc evaporation of graphite) have been compared.[147] In Figure 39, we show the temperature dependence of magnetic

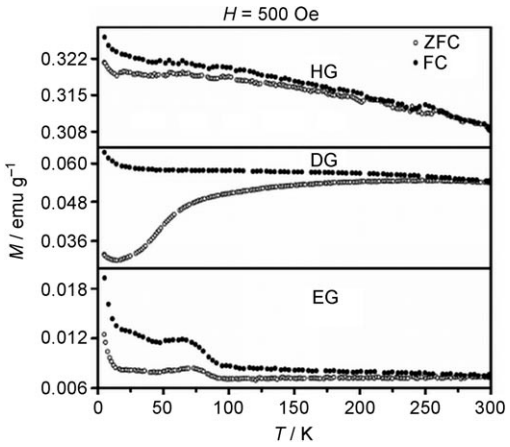

Figure 39. Temperature dependence of the magnetic moment of graphenes (EG, DG, HG) at a field of 500 Oe. (From Ref. [147].)

susceptibility for the three samples. The graphenes show Cuire–Weiss type behavior, similar to activated carbon fibers, with a negative Weiss temperature. There is divergence between field-cooled (FC) and zero-field-cooled (ZFC) data at low fields, this divergence disappears at high fields. Furthermore, there is magnetic hysteresis at 300 K. Typical hysteresis curves of the three samples are shown in Figure 40. The magnetization decreases markedly on adsorption of electron-donor molecules. HG shows the highest magnet-

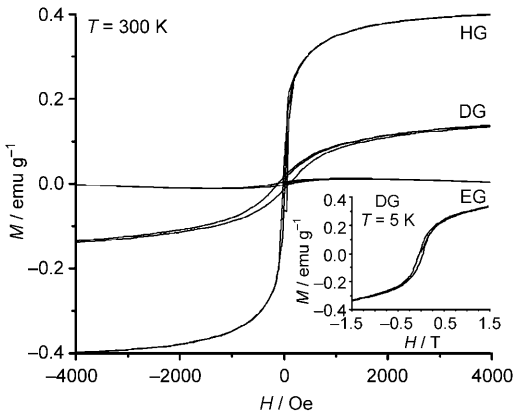

Figure 40. Magnetisation (M) versus filed strength (H) hysteresis loops of different graphene samples (EG, DG, and HG) measured at 300 K. Inset: hysteresis loop at 5 K. (From Ref. [147].)

ization and Weiss temperature. It is noteworthy that HG has the smallest number of layers and also the smallest surface area thus indicating that edge states and/or defects play a role. AC susceptibility data do not show any frequency dependence thus ruling out spin-glass behavior in these graphene samples. It appears that antiferromagnetic and ferromagnetic interactions coexist in graphene, with the ferromagnetic clusters growing with increasing applied magnetic field. Clearly, more detailed studies on the magnetic properties of well-characterized graphene samples are necessary, and it is essential to ensuring that there are absolutely no magnetic impurities in the sample. The electronic and magnetic properties of graphene would be affected by depositing magnetic nanoparticles and this aspect also requires further study.

8.2. Electrical and Electrochemical Properties

Few-layer graphenes and nanographite particles show semiconducting or insulating behavior with their resistance showing little change in the range 100–300 K. The resistivity increases sharply below 50 K and decreases markedly if the graphene is heated to high temperatures. Thus, graphene nanoribbons obtained from exfoliation of graphite show semiconducting properties. Graphene nanoribbons are predicted to be half-metallic. This behavior should be realizable if in-plane homogeneous electric fields are applied across zigzag edges.[142d] Graphene sheets prepared from graphite oxide show well-behaved field-effect transistor (FET) properties.[29a,14a] The charge carrier mobility for electrons and holes is of the order 10 $cm^2 V^{-1} s^{-1}$.[148,149] It is remarkable that field-effect transistor properties are found even though the samples have defects. FETs have been fabricated with nanoribbons with an on–off ratio of 10^7 at room tempereature.[150] The nanoribbon (less than 10 nm wide) FETs exhibit properties comparable to carbon nanotubes (CNTs).[151] The saturation velocity of graphene FETs depends on the charge-carrier concentration, this dependence is because of the scattering of interfacial phonons in the silica layer.[152] Electrostatic modulation gives rise to transconductances as high as 150 $\mu S\,\mu m^{-1}$.[152]

Fabrication of graphene-based transparent and conductive thin films has been carried out by thermal reduction of graphite oxide.[153] These films are similar to HOPG in their electronic and structural properties. Reaction with atomic hydrogen transforms graphene, which is a conductive zero-overlap semimetal, into an insulator.[154] The reaction is reversible and the original properties of graphene are restored on annealing.

The optical conductivity of graphene has been measured on a silica substrate for photon energies between 0.2 and 1.2 eV and the properties explained on the basis of non-interacting massless Dirac fermions.[155] Graphene nanoribbons appear to exhibit high magnetoresistance, which may enable the design of spin-valve devices.[156] Recently, the room-temperature thermal conductivity of graphene has been measured by using a non-contact optical-based technique. It has shown that the conductivity reaches values of up to $(5.30 \pm 0.48) \times 10^3\ W\,mK^{-1}$.[157]

A graphene-based superconducting transistor has been reported.[158] Although graphene is not superconducting by itself, when placed between superconducting electrodes it shows supercurrents over short distances because of the Josephson effect. By employing the non-equilibrium Green's function method, the transmission of superconductor–graphene–superconductor junctions has been examined theoretically.[159] Palladium sheets sandwiched between graphene sheets give rise to a superconducting transition around 3.6 K.[160] In this case the superconductivity occurs in the palladium sheets.

The electrochemical properties of different graphenes (EG, DG, and CG, see above for definitions) have been investigated using the redox reactions with potassium ferrocyanide. Out of the three graphenes, EG shows a behavior similar to the basal plane in graphite whereas DG and CG show slightly faster kinetics.[47,1d] Vivekchand et al.[161] have investigated different graphene samples as electrode materials for electrochemical supercapacitors using aq. H_2SO_4 and an ionic liquid (*N*-butyl-*N*-methylpyrrolidinium bis(trifluoromethanesulfonyl)imide; $PYR_{14}TFSI$) as electrolytes.[161,1d] EG and DG exhibit high specific capacitance in aq. H_2SO_4, with the values reaching up to 117 and 35 $F\,g^{-1}$, respectively. The voltammetric characteristics of a capacitor built from graphene electrodes (5 mg each) in aqueous H_2SO_4 (1 M) is shown in Figure 41 a and b. By using the ionic liquid, the operating voltage can be extended to 3.5 V (instead of 1 V in the case of aq. H_2SO_4), the specific capacitance values are 75 and 40 $F\,g^{-1}$ for EG and DG, respectively. In aqueous medium, high-surface-area graphite prepared by ball-milling showed a large specific capacitance of 33 $\mu F\,cm^{-2}$, which might be due to the large open surface area, lattice defects, and oxygen functional groups present in the sample.[162]

Chemically modified graphene sheets obtained by the reduction of graphene oxide with hydrazine have also been

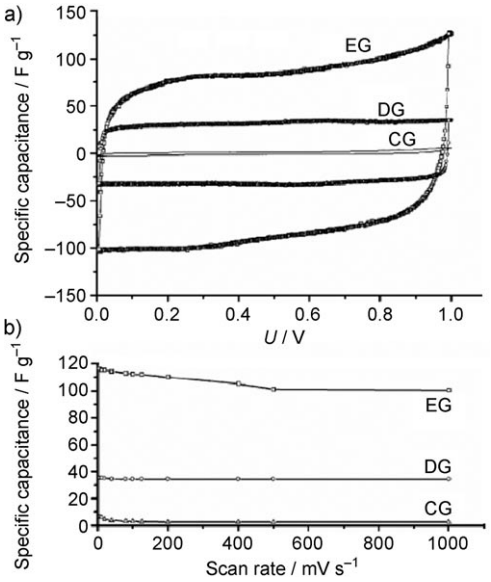

Figure 41. a) Voltammetric characteristics of a capacitor built from different graphene electrodes (5 mg each) at a scan rate of 100 $mV\,s^{-1}$ in aqueous H_2SO_4 (1 M) and b) specific capacitance as a function of scan rate. (From Ref. [161].)

investigated as electrode materials in supercapacitors.[163] Graphene nanosheets show a high lithium-storage capacity, with values reaching 540 mAh g^{-1}, which is interesting for lithium secondary batteries. By incorporating CNTs and C_{60} this value can be extended up to 730 mAh g^{-1} and 784 mAh g^{-1}, respectively.[164] Photovoltaic devices have been fabricated with a bulk hetero-junction (BHJ) architecture by employing solution-processible graphene as an electron-acceptor material. A power conversion efficiency of 14% is obtained using simulated 100 mW cm^{-2} AM 1.5 G illumination.[165] The optical transparency and conductivity of graphene can be exploited for many photonic devices. Thus, liquid-crystal devices with electrodes made of graphene show excellent performance with a high contrast ratio.[166] Conducting films of graphene for solar-cell applications can also be prepared by a bottom-up approach.[167a] Polymer photovoltaic cells based on solution-processable graphene have been reported.[167b]

8.3. Surface and Sensor Properties

Single-layer graphene is predicted to have a large surface area close to 2600 m^2 g^{-1}.[168] Surface areas of different few-layer graphene samples have been measured by the Brunauer–Emmett–Teller (BET) method and are in the range of 270–1550 m^2 g^{-1}. Thus, few-layer graphenes show large surface areas, some of them approaching the value of single layer graphene.

Hydrogen-uptake data of different graphene samples have been reported.[169] In Figure 42a, H_2 adsorption and desorption curves of the EG are shown. H_2 adsorption measurements at 1 atm and 77 K show that DG, EG, and HG can absorb 1.2, 1.7, and 1.0 wt%, respectively, of H_2. These samples show higher uptakes at 100 bar and 300 K, the values being 2.5, 3.1, and 2.0 wt% for DG, EG, and HG, respectively. The adsorption is completely reversible and comparable to that of carbon nanotubes[170] and porous open-framework materials.[180] The values of the H_2 uptake at 1 atm and 77 K by the various graphene samples vary linearly with the surface area. By extrapolation of the linear plot to the surface area of single-layer graphene, we estimate its H_2 uptake to be around 3 wt% at 1 atm and 77 K. Though the H_2 uptake of graphenes are low compared to the 6.0 wt% target of the US Department of Energy, there is scope for significant improvement, by producing samples with a smaller number of layers and higher surface areas. It is possible that single layer graphene will exhibit 5–6 wt% of H_2 uptake at 100 atm and 300 K. First-principles calculations show that the H_2 molecules sit alternately parallel and perpendicular to the six-membered rings of graphene layer and that single-layer graphene can accommodate up to 7.7 wt% of hydrogen.[169]

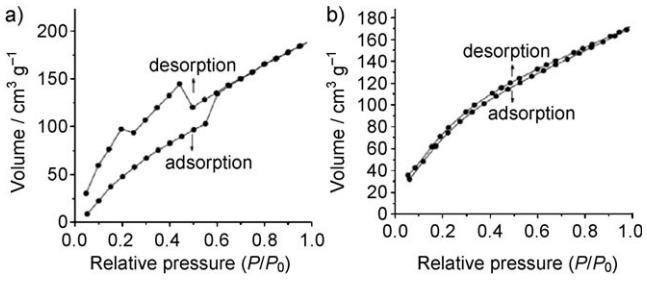

Figure 42. a) H_2 adsorption isotherms of EG at 1 atm and 77 K. b) CO_2 adsorption isotherms of EG at 1 atm and 195 K. (From Ref. [169].)

The uptake of CO_2 by few-layer graphenes at 1 atm and 195 K is found to go up to around 35 wt%. Figure 42b shows typical CO_2 adsorption and desorption curves of the EG sample. First-principles calculations show that CO_2 molecules sit alternately in a parallel fashion on the six-membered rings giving a maximum uptake of 37.9 wt% in the case of single-layer graphene.[169] Employing first-principles calculations, adsorption of different gas molecules (CO, NO, NO_2, O_2, N_2, CO_2, and NH_3) on graphene nanoribbons has been studied.[172,110] It is shown that NH_3 can modify the conductance of the nanoribbons, while other gas molecules have little effect. This property can be used to detect NH_3 in a mixture of the other gases.[171]

Gas-sensor properties of graphene have been examined by a few groups. For example, it has been shown that mechanically exfoliated graphene flakes can detect a single molecule of NO_2.[173] Rangel et al.[174] theoretically predict the potential application of graphene acting as a sensor of single molecules. Reduced graphene oxide has been shown to be a good sensor achieving sensitivities at parts-per-billion levels for chemical warfare agents and explosives.[175] By adjusting the reduction process, the response and recovery characteristics of the conductance response can be tailored. Sensitivity of chemically converted graphene for the detection of NO_2, NH_3, and dinitrotoluene has been investigated.[176] The primary mechanism of the chemical response is charge transfer, the electrical contacts play only a limited role. DFT calculations show that aluminum-doped graphene strongly chemisorbs CO molecules forming Al-CO bonds, thus aluminum-doped graphene is expected to be a potential candidate for the detection of CO.[177]. Ghosh et al.[178] have studied the sensor characteristics of thick films made of few-layer graphenes for NO_2, H_2O, and aliphatic alcohols. Good sensitivities for NO_2 and H_2O have been found and the sensitivity is affected by boron or nitrogen doping. Chemically modified graphene has been used in bioelectronics as a sensor at both the microbial and the molecular level.[179] It can act as an interface to recognize single bacteria, a label-free, reversible DNA detector, and a polarity-specific molecular transistor for protein/DNA adsorption. The gas-sensing properties of graphene sheets deposited on $LiTaO_3$ substrates have been investigated.[180] The possibilities of single-layer graphene to act as a mass sensor and an atomic dust detector have also been indicated.[181] Glucose sensors based on graphene have been reported.[182a,b] FETs of solution-gated epitaxial graphene can be used as a pH sensor.[182c]

8.4. Binding of DNA Nucleobases and Nucleosides

By employing isothermal titration calorimetry, Varghese et al.[183] have investigated the interaction of graphene with DNA nucleobases and nucleosides. The order of interaction

energies of the nucleobases varies as guanine (G) > adenine (A) > cytosine (C) ≈ thymine (T) in aqueous solution, the positions of C and T seem to be interchangeable. Nucleosides also follow the same trend and the interaction energies of A–T and G–C pairs are somewhere between those of the constituent bases. Theoretical calculations including van der Waals interaction and solvation energy give the trend as G > A ≈ T > C.

9. Polymer Composites

There has been some significant work on graphene–polymer composites. Processing of nanographene platelets to produce composites has been briefly reviewed by Jang et al.[184a] Polyacrylonitrile nanofibers reinforced by graphite nanoplatelets have been prepared and have improved mechanical properties.[184b] Hansma et al.[185] indicated how a combination of adhesives and high-strength structures such as graphene and carbon nanotubes can yield strong, light-weight, and damage-resistant materials. Ramanathan et al.[186] reported that 1 wt% of functionalized graphene sheets in poly(acrylonitrile) increases the glass transition temperature (T_g) of the polymer by over 40 °C and an increase of nearly 30 °C is observed with only 0.05 wt% of graphene in poly(methyl methacrylate) (PMMA). An addition of approximately 1 wt% of graphene to PMMA leads to increases in the elastic modulus by 80% and in the ultimate tensile strength by 20%. A comparative study by these workers shows that among all the nano-filler materials considered, single-layer functionalized graphene gives the best results. Das et al.[187] have studied the mechanical properties of polyvinyl alcohol (PVA) and PMMA composites reinforced by functionalized few-layer graphene by employing the nano-indentation technique. The addition of 0.6 wt% of the graphene results in as significant increase in both the elastic modulus and hardness (Figure 43). The crystallinity of PVA also increases with the addition of few-layer graphene. The observed improvement in the mechanical properties of the polymers is suggested to arise from the good mechanical interaction between the polymer and the few-layer graphene which in turn provides better load-transfer between the matrix and the fiber.

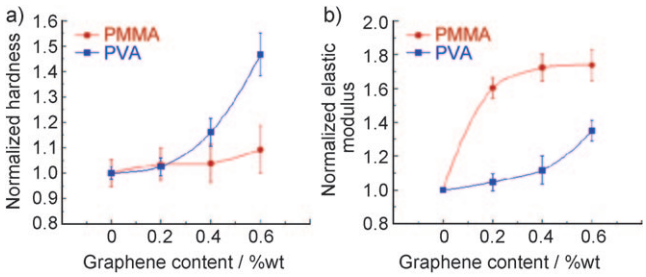

Figure 43. Normalized a) hardness (*H*) and b) elastic modulus (*E*) plotted as a function of graphene content for PVA and PMMA composites. (The pristine values of PMMA and PVA are E_{PMMA} = 2.1 GPa, H_{PMMA} = 140 MPa, E_{PVA} = 0.65 GPa, and H_{PVA} = 38 MPa). (From Ref. [187].)

Epoxy composites of few-layer graphene show very interesting properties which are useful for the development of thermal interface materials for electronic packaging and advanced composites.[188] A loading of nearly 25 vol% of graphene into epoxy matrix enhances the thermal conductivity by more than 3000%, which surpasses the performance of conventional fillers which require a loading of nearly 70 vol% to achieve this value. A graphene–C_{60} hybrid material has been synthesized by chemically coupling graphene oxide and pyrrolidine fullerene.[189] Graphene membranes of 100 μm diameter have been prepared.[190] They exhibit high stiffness and support large loads. An atomic simulation has been employed to investigate the elastic properties of single-layer graphene.[191] Metal nanoparticles have been mechanically entrapped between graphene sheets to facilitate better contact between the particles and the polymer matrix.[192]

Transparent and electrically conductive graphene–silica composite films were fabricated by employing a simple sol–gel route. In this process, graphene oxide sheets are incorporated into silica sols followed by spin-coating, chemical reduction, and thermal curing.[193] Polystyrene–graphene composites exhibit a percolation threshold of 0.1 V% for room temperature electrical conductivity, with a conductivity of 0.1 S m^{-1} at only 1 V%.[55] Electrically conducting graphene paper is not only biocompatible but also mechanically strong.[194] The paper is prepared by the directional flow-induced assembly of graphene sheets dispersed in solution.

10. Outlook

Herein we have highlighted the important aspects of the chemistry of graphene which have attracted attention in the last two to three years. Many challenges remain, the ability to synthesize graphenes with the desired number of layers on a large scale being the foremost. We still need exact methods for the synthesis just as we need exact procedures for definitive characterization of graphenes with different numbers of layers. Many properties of graphene are not fully understood, magnetic properties being one of them. Magnetic properties of samples have to be measured after ensuring that there is absolutely no trace of magnetic impurities. Changes in the various properties of graphene with the number of layers need to be investigated.

There are indications that some applications of graphenes are possible, sensors, transistors and solar cells being examples. The extraordinary sensitivity of the electronic structure of graphene to doping and such characteristics should be useful in certain applications. The mechanical properties of graphene–polymer composites containing other additives, such as carbon nanotubes, could be of great interest. The toxicological aspects of different graphene samples need to be examined. Modified graphenes (e.g., graphenes in which carbon atoms are replaced extensively by boron or silicon atoms) as well as inorganic graphenes formed by layered materials, such as MoS_2, are likely to be rich areas for investigation.

An interesting question arises if silicene, a monolayer of silicon atoms tightly packed into a two-dimensional honey-

comb lattice, exists. If it does, it will reveal fascinating new physics and will be an excellent candidate for nanoelectronics, smoothly integrating with the present silicon microtechnology. A recent report by Kara et al.[195] claims to have achieved epitaxial growth of silicene stripes self-aligned in a parallel array on an anisotropic silver (110) surface. These results are yet to be reproduced by other groups. In the meantime, Sheka,[196] based on quantum-chemical calculations, has argued against the existence of silicene. It will be exciting to see if silicene does exist.

Received: March 27, 2009
Published online: September 22, 2009

[1] a) A. K. Geim, K. S. Novoselov, *Nat. Mater.* **2007**, *6*, 183; b) D. Li, R. B. Kaner, *Science* **2008**, *320*, 1170; c) M. I. Katsnelson, *Mater. Today* **2007**, *10*, 20; d) C. N. R. Rao, K. Biswas, K. S. Subrahmanyam, A. Govindaraj, *J. Mater. Chem.* **2009**, *19*, 2457.
[2] K. S. Novoselov, A. K. Geim, S. V. Morozov, D. Jiang, M. I. Katsnelson, I. V. Grigorieva, S. V. Dubonos, A. A. Firsov, *Nature* **2005**, *438*, 197.
[3] Y. Zhang, J. W. Tan, H. L. Stormer, P. Kim, *Nature* **2005**, *438*, 201.
[4] K. S. Novoselov, Z. Jiang, Y. Zhang, S. V. Morozov, H. L. Stormer, U. Zeitler, J. C. Maan, G. S. Boebinger, P. Kim, A. K. Geim, *Science* **2007**, *315*, 1379.
[5] K. S. Novoselov, A. K. Geim, S. V. Morozov, D. Jiang, Y. Zhang, S. V. Dubonos, I. V. Grigorieva, A. A. Firsov, *Science* **2004**, *306*, 666.
[6] M. Y. Han, B. Oezyilmaz, Y. Zhang, P. Kim, *Phys. Rev. Lett.* **2007**, *98*, 206805.
[7] C. Lee, X. Wei, J. W. Kysar, J. Hone, *Science* **2008**, *321*, 385.
[8] S. Park, R. S. Ruoff, *Nat. Nanotechnol.* **2009**, *4*, 217.
[9] a) K. S. Novoselov, D. Jiang, F. Schedin, T. J. Booth, V. V. Khotkevich, S. V. Morozov, A. K. Geim, *Proc. Natl. Acad. Sci. USA* **2005**, *102*, 10451; b) P. Blake, E. W. Hill, A. H. C. Neto, K. S. Novoselov, D. Jiang, R. Yang, T. J. Booth, A. K. Geim, *Appl. Phys. Lett.* **2007**, *91*, 063124.
[10] S. Roddaro, P. Pingue, V. Piazza, V. Pellegrini, F. Beltram, *Nano Lett.* **2007**, *7*, 2707.
[11] E. Stolyarova, R. K. Taeg, S. Ryu, J. Maultzsch, P. Kim, L. E. Brus, T. F. Heinz, M. S. Hybertsen, G. W. Flynn, *Proc. Natl. Acad. Sci. USA* **2007**, *104*, 9209.
[12] a) J. C. Meyer, A. K. Geim, M. I. Katsnelson, K. S. Novoselov, T. J. Booth, S. Roth, *Nature* **2007**, *446*, 60; b) J. C. Meyer, C. Kisielowski, R. Erni, M. D. Rossell, M. F. Crommie, A. Zettl, *Nano Lett.* **2008**, *8*, 3582.
[13] a) A. Gupta, G. Chen, P. Joshi, S. Tadigadapa, P. C. Eklund, *Nano Lett.* **2006**, *6*, 2667; b) A. C. Ferrari, *Solid State Commun.* **2007**, *143*, 47.
[14] A. C. Ferrari, J. C. Meyer, V. Scardaci, C. Casiraghi, M. Lazzeri, F. Mauri, S. Piscanec, D. Jiang, K. S. Novoselov, S. Roth, A. K. Geim, *Phys. Rev. Lett.* **2006**, *97*, 187401.
[15] M. A. Pimenta, G. Dresselhaus, M. S. Dresselhaus, L. A. Cancado, A. Jorio, R. Sato, *Phys. Chem. Chem. Phys.* **2007**, *9*, 1276.
[16] D. Graf, F. Molitor, K. Ensslin, C. Stampfer, A. Jungen, C. Hierold, L. Wirtz, *Nano Lett.* **2007**, *7*, 238.
[17] K. A. Ritter, J. L. Lyding, *Nanotechnology* **2008**, *19*, 015704.
[18] A. N. Sidorov, M. M. Yazdanpanah, R. Jalilian, P. J. Ouseph, R. W. Cohn, G. U. Sumanasekera, *Nanotechnology* **2007**, *18*, 135301.
[19] E. Rollings, G.-H. Gweon, S. Y. Zhou, B. S. Mun, J. L. McChesney, B. S. Hussain, A. V. Fedorov, P. N. First, W. A. de Heer, A. Lanzara, *J. Phys. Chem. Solids* **2006**, *67*, 2172.
[20] a) C. Virojanadara, M. Syväjarvi, R. Yakimova, L. I. Johansson, *Phys. Rev. B* **2008**, *78*, 245403; b) K. V. Emtsev, A. Bostwick, K. Horn, J. Jobst, G. L. Kellogg, L. Ley, J. L. McChesney, T. Ohta, S. A. Reshanov, J. Rohrl, E. Rotenberg, A. K. Schmid, D. Waldmann, H. B. Weber, T. Seyller, *Nat. Mater.* **2009**, *8*, 203; c) K. Kim, H. Lee, J. Choi, H. K. Lee, T. Kang, B. Kim, S. Kim, *J. Phys. Condens. Matter* **2008**, *20*, 225017.
[21] a) M. Lotya, Y. Hernandez, P. J. King, R. J. Smith, V. Nicolosi, L. S. Karlsson, F. M. Blighe, S. De, Z. Wang, I. T. McGovern, G. S. Duesberg, J. N. Coleman, *J. Am. Chem. Soc.* **2009**, *131*, 3611; b) X. Lu, M. Yu, H. Huang, R. S. Ruoff, *Nanotechnology* **1999**, *10*, 269.
[22] A. G. Cano-Marquez, F. J. Rodríguez-Macias, J. Campos-Delgado, C. G. Espinosa-Gonzalez, F. Tristan-Lopez, D. Ramírez-Gonzalez, D. A. Cullen, D. J. Smith, M. Terrones, Y. I. Vega-Cantu, *Nano Lett.* **2009**, *9*, 1527.
[23] M. Choucair, P. Thordarson, J. A. Stride, *Nat. Nanotechnol.* **2009**, *4*, 30.
[24] Y. Hernandez, V. Nicolosi, M. Lotya, F. M. Blighe, Z. Sun, S. De, I. T. Mcgovern, B. Holland, M. Byrne, Y. K. Gun′ko, J. J. Boland, P. Niraj, G. Duesberg, S. Krishnamurthy, R. Goodhue, J. Hutchison, V. Scardaci, A. C. Ferrari, J. N. Coleman, *Nat. Nanotechnol.* **2008**, *3*, 563.
[25] C. Vallés, C. Drummond, H. Saadaoui, C. A. Furtado, M. He, O. Roubeau, L. Ortolani, M. Monthioux, A. Penicaud, *J. Am. Chem. Soc.* **2008**, *130*, 15802.
[26] X. Yang, X. Dou, A. Rouhanipour, L. Zhi, H. J. Rader, K. Müllen, *J. Am. Chem. Soc.* **2008**, *130*, 4216.
[27] X. Li, G. Zhang, X. Bai, X. Sun, X. Wang, E. Wang, H. Dai, *Nat. Nanotechnol.* **2008**, *3*, 538.
[28] a) S. Park, J. An, I. Jung, R. D. Piner, S. J. An, X. Li, A. Velamakanni, R. S. Ruoff, *Nano Lett.* **2009**, *9*, 1593; b) D. Li, M. B. Muller, S. Gilje, R. B. Kaner, G. D. Wallace, *Nat. Nanotechnol.* **2008**, *3*, 101.
[29] a) V. C. Tung, M. J. Allen, Y. Yang, R. B. Kaner, *Nat. Nanotechnol.* **2009**, *4*, 25; b) H. C. Schniepp, J. L. Li, M. J. McAllister, H. Sai, M. Herrera-Alonso, D. H. Adamson, R. K. Prud′homme, R. Car, D. A. Saville, I. A. Aksay, *J. Phys. Chem. B* **2006**, *110*, 8535; c) M. J. McAllister, J.-L. Li, D. H. Adamson, H. C. Schniepp, A. A. Abdala, J. Liu, M. H. -Alonso, D. L. Milius, R. Car, R. K. Prud′homme, I. A. Aksay, *Chem. Mater.* **2007**, *19*, 4396.
[30] J. I. Paredes, S. Villar-Rodil, A. Martinez-Alonso, J. M. D. Tascon, *Langmuir* **2008**, *24*, 10560.
[31] A. Dato, V. Radmilovic, Z. Lee, J. Phillips, M. Frenklach, *Nano Lett.* **2008**, *8*, 2012.
[32] G. D. Yuan, W. J. Zhang, Y. Yang, Y. B. Tang, Y. Q. Li, J. X. Wang, X. M. Meng, Z. B. He, C. M. L. Wu, I. Bello, C. S. Lee, S. T. Lee, *Chem. Phys. Lett.* **2009**, *467*, 361.
[33] Z. Wu, W. Ren, L. Gao, B. Liu, C. Jiang, H. Cheng, *Carbon* **2009**, *47*, 493.
[34] A. Reina, H. Son, L. Jiao, B. Fan, M. S. Dresselhaus, Z. F. Liu, J. Kong, *J. Phys. Chem. C* **2008**, *112*, 17741.
[35] A. N. Obraztsov, E. A. Obraztsova, A. V. Tyurnina, A. A. Zolotukhin, *Carbon* **2007**, *45*, 2017.
[36] a) K. S. Subrahmanyam, L. S. Panchakarla, A. Govindaraj, C. N. R. Rao, *J. Phys. Chem. C* **2009**, *113*, 4257; b) Z.-S. Wu, W. Ren, L. Gao, J. Zhao, Z. Chen, B. Liu, D. Tang, B. Yu, C. Jiang, H.-M. Cheng, *ACS Nano* **2009**, *3*, 411.
[37] X. K. Wang, X. W. Lin, M. Mesleh, M. F. Jarrold, V. P. Dravid, J. B. Ketterson, R. P. H. Chang, *J. Mater. Res.* **1995**, *10*, 1977.
[38] X. K. Wang, X. W. Lin, V. P. Dravid, J. B. Ketterson, R. P. H. Chang, *Appl. Phys. Lett.* **1995**, *66*, 2430.
[39] R. Seshadri, A. Govindaraj, H. N. Aiyer, R. Sen, G. N. Subbanna, A. R. Raju, C. N. R. Rao, *Curr. Sci.* **1994**, *66*, 839.

[40] A. Malesevic, R. Vitchev, K. Schouteden, A. Volodin, L. Zhang, G. V. Tendeloo, A. Vanhulsel, C. V. Haesendonck, *Nanotechnology* **2008**, *19*, 305604.
[41] A. Reina, X. Jia, J. Ho, D. Nezich, H. Son, V. Bulovic, M. S. Dresselhaus, J. Kong, *Nano Lett.* **2009**, *9*, 30.
[42] J. Campos-Delgado, J. M. Romo-Herrera, X. Jia, D. A. Cullen, H. Muramatsu, Y. A. Kim, T. Hayashi, Z. Ren, D. J. Smith, Y. Okuno, T. Ohba, H. Kanoh, K. Kaneko, M. Endo, H. Terrones, M. S. Dresselhaus, M. Terrones, *Nano Lett.* **2008**, *8*, 2773.
[43] N. G. Shang, P. Papakonstantinou, M. McMullan, M. Chu, A. Stamboulis, A. Potenza, S. S. Dhesi, H. Marchetto, *Adv. Funct. Mater.* **2008**, *18*, 3506.
[44] S. Gilje, S. Han, M. Wang, K. L. Wang, R. B. Kaner, *Nano Lett.* **2007**, *7*, 3394.
[45] Y. Xu, H. Bai, G. Lu, C. Li, G. Shi, *J. Am. Chem. Soc.* **2008**, *130*, 5856.
[46] G. Wang, J. Yang, J. Park, X. Gou, B. Wang, H. Liu, J. Yao, *J. Phys. Chem. C* **2008**, *112*, 8192.
[47] K. S. Subrahmanyam, S. R. C. Vivekchand, A. Govindaraj, C. N. R. Rao, *J. Mater. Chem.* **2008**, *18*, 1517.
[48] P. R. Somani, S. P. Somani, M. Umeno, *Chem. Phys. Lett.* **2006**, *430*, 56.
[49] O. E. Andersson, B. L. V. Prasad, H. Sato, T. Enoki, Y. Hishiyama, Y. Kaburagi, M. Yoshikawa, S. Bandow, *Phys. Rev. B* **1998**, *58*, 16387.
[50] V. Huc, N. Bendiab, N. Rosman, T. Ebbesen, C. Delacour, V. Bouchiat, *Nanotechnology* **2008**, *19*, 455601.
[51] a) K. S. Kim, Y. Zhao, H. Jang, S. Y. Lee, J. M. Kim, K. S. Kim, J. Ahn, P. Kim, J. Choi, B. H. Hong, *Nature* **2009**, *457*, 706; b) W. Cai, R. D. Piner, F. J. Stadermann, S. Park, M. A. Shaibat, Y. Ishii, D. Yang, A. Velamakanni, S. J. An, M. Stoller, J. An, D. Chen, R. S. Ruoff, *Science* **2008**, *321*, 1815; c) P. W. Sutter, J. Flege, E. A. Sutter, *Nat. Mater.* **2008**, *7*, 406; d) P. Yi, S. Dong-Xia, G. Hong-Jun, *Chin. Phys.* **2007**, *16*, 3151; e) H. J. Räder, A. Rouhanipour, A. M. Talarico, V. Palermo, P. Samori, K. Müllen, *Nat. Mater.* **2006**, *5*, 276.
[52] D. A. Dikin, S. Stankovich, E. J. Zimney, R. D. Piner, G. H. B. Dommett, G. Evmenenko, S. T. Nguyen, R. S. Ruoff, *Nature* **2007**, *448*, 457.
[53] L. Staudenmaier, *Ber. Dtsch. Chem. Ges.* **1898**, *31*, 1481.
[54] X. Fan, W. Peng, Y. Li, X. Li, S. Wang, G. Zhang, F. Zhang, *Adv. Mater.* **2008**, *20*, 4490.
[55] S. Stankovich, D. A. Dikin, G. H. B. Dommett, K. M. Kohlhaas, E. J. Zimney, E. A. Stach, R. D. Piner, S. T. Nguyen, R. S. Ruoff, *Nature* **2006**, *442*, 282.
[56] a) S. Stankovich, R. D. Piner, X. Q. Chen, N. Q. Wu, S. T. Nguyen, R. S. Ruoff, *J. Mater. Chem.* **2006**, *16*, 155; b) S. Stankovich, D. A. Dikin, R. D. Piner, K. A. Kohlhaas, A. Kleinhammes, Y. Jia, Y. Wu, S. T. Nguyen, R. S. Ruoff, *Carbon* **2007**, *45*, 1558.
[57] Y. Liang, D. Wu, X. Feng, K. Müllen, *Adv. Mater.* **2009**, *21*, 1679.
[58] See, for example, R. Saito, G. Dresselhaus, M. S. Dresselhaus, *Physical Properties of Carbon Nanotubes*, Imperial College Press, London, **1998**.
[59] A. H. Castro Neto, F. Guinea, N. M. R. Peres, K. S. Novoselov, A. K. Geim, *Rev. Mod. Phys.* **2009**, *81*, 109.
[60] M. I. Katsnelson, K. S. Novoselov, A. K. Geim, *Nat. Phys.* **2006**, *2*, 620.
[61] P. Gosselin, A. Berard, H. Mohrbach, S. Ghosh, *Eur. Phys. J. C* **2009**, *59*, 883.
[62] E. McCann, V. I. Falko, *Phys. Rev. Lett.* **2006**, *96*, 086805.
[63] H. Min, B. R. Sahu, S. K. Bannerji, A. H. MacDonald, *Phys. Rev. B* **2007**, *75*, 155115.
[64] T. Ohta, A. Bostwick, T. Seyller, K. Horn, E. Rotenberg, *Science* **2006**, *313*, 951.
[65] J. B. Oostinga, H. B. Heersche, X. Liu, A. F. Morpurgo, L. M. K. Vandersypen, *Nat. Mater.* **2008**, *7*, 151.
[66] Z. Jiang, Y. Zhang, Y. W. Tan, H. L. Stormer, P. Kim, *Solid State Commun.* **2007**, *143*, 14.
[67] K. S. Novoselov, E. McCann, S. V. Morozov, V. I. Falko, M. I. Katsnelson, U. Zeitler, D. Ziang, F. Schedin, A. K. Geim, *Nat. Phys.* **2006**, *2*, 177.
[68] E. V. Castro, K. S. Novoselov, S. V. Morozov, N. M. R. Peres, J. M. B. Lopes dos Santos, J. Nilsson, F. Guineau, A. K. Geim, A. H. Castro Neto, *Phys. Rev. Lett.* **2007**, *99*, 216802.
[69] S. Reich, C. Thomsen, *Philos. Trans. R. Soc. London Ser. A* **2004**, *362*, 2271.
[70] J. A. Yan, W. Y. Ruan, M. Y. Chou, *Phys. Rev. B* **2008**, *77*, 125401.
[71] S. K. Saha, U. V. Waghmare, H. R. Krishnamurthy, A. K. Sood, *Phys. Rev. B* **2008**, *78*, 165421.
[72] a) S. Piscanec, M. Lazzeri, F. Mauri, A. C. Ferrari, J. Robertson, *Phys. Rev. Lett.* **2004**, *93*, 185503; b) O. Dubay, G. Kresse, *Phys. Rev. B* **2003**, *67*, 035401.
[73] S. Piscanec, M. Lazzeri, J. Robertson, A. C. Ferrari, F. Mauri, *Phys. Rev. B* **2007**, *75*, 035427.
[74] M. Lazzeri, F. Mauri, *Phys. Rev. Lett.* **2006**, *97*, 266407.
[75] C. H. Park, F. Giustino, M. L. Cohen, S. G. Louie, *Nano Lett.* **2008**, *8*, 4229.
[76] A. H. Castro Neto, F. Guinea, *Phys. Rev. B* **2007**, *75*, 045404.
[77] J. Yan, W. Y. Ran, M. Y. Chou, *arXiv.org e-Print Arch. Condens. Matter* **2009**, arXiv:0901.3086.
[78] W. Kohn, *Phys. Rev. Lett.* **1959**, *2*, 393.
[79] D. M. Basko, *arXiv.org e-Print Arch. Condens. Matter* **2009**, arXiv:0902.4345.
[80] A. Das, B. Chakraborty, A. K. Sood, *Bull. Mater. Sci.* **2008**, *31*, 579.
[81] C. Casiraghi, S. Pisana, K. S. Novoselov, A. K. Geim, A. C. Ferrari, *Appl. Phys. Lett.* **2007**, *91*, 233108.
[82] C. Stampfer, F. Molitor, D. Graf, K. Ensslin, A. Jungen, C. Hierold, L. Wirtz, *Appl. Phys. Lett.* **2007**, *91*, 241907.
[83] Z. Ni, Y. Wang, T. Yu, Z. X. Shen, *Nano Res.* **2008**, *1*, 273.
[84] C. Thomsen, S. Reich, *Phys. Rev. Lett.* **2000**, *85*, 5214.
[85] A. K. Sood, R. Gupta, C. H. Munro, S. A. Asher in *Proceedings of the XVI International Conference on Raman Spectroscopy* (Ed.: A. M. Heyns), Wiley, Chichester, p. 62.
[86] A. K. Sood, R. Gupta, S. A. Asher, *J. Appl. Phys.* **2001**, *90*, 4494.
[87] a) D. M. Basko, *Phys. Rev. B* **2007**, *76*, 081405; b) D. M. Basko, *Phys. Rev. B* **2008**, *78*, 125418.
[88] Y. You, Z. Ni, T. Yu, Z. X. Shen, *Appl. Phys. Lett.* **2008**, *93*, 163112.
[89] J. Rohrl, M. Hundhausen, K. V. Emtsev, T. Seyller, R. Graupner, L. Ley, *Appl. Phys. Lett.* **2008**, *92*, 201918.
[90] N. Ferralis, R. Maboudian, C. Carraro, *Phys. Rev. Lett.* **2008**, *101*, 156801.
[91] Z. H. Ni, W. Chen, X. F. Fan, J. L. Kuo, T. Yu, A. T. S. Wee, Z. X. Shen, *Phys. Rev. B* **2008**, *77*, 115416.
[92] T. M. G. Mohiuddin, A. Lombardo, R. R. Nair, A. Bonetti, G. Savini, R. Jalil, N. Bonini, D. M. Basko, C. Galiotis, N. Marzari, K. S. Novoselov, A. K. Geim, A. C. Ferrari, *arXiv.org e-Print Arch. Condens. Matter* **2008**, arXiv:0812.1538.
[93] M. Huang, H. Yan, J. Hone, C. Chen, D. Song, T. F. Heinz, *arXiv.org e-Print Arch. Condens. Matter* **2008**, arXiv:0812.225.
[94] T. Yu, Z. Ni, C. Du, Y. You, Y. Wang, Z. X. Shen, *J. Phys. Chem. C* **2008**, *112*, 12602.
[95] Z. H. Ni, H. M. Wang, Y. Ma, J. Kasim, Y. H. Wu, Z. X. Shen, *ACS Nano* **2008**, *2*, 1033.
[96] S. Pisana, M. Lazzeri, C. Casiraghi, K. S. Novoselov, A. K. Geim, A. C. Ferrari, F. Mauri, *Nat. Mater.* **2007**, *6*, 198.
[97] J. You, Y. Zhang, P. Kim, A. Pinczuk, *Phys. Rev. Lett.* **2007**, *98*, 166802.
[98] A. Das, A. K. Sood, A. Govindaraj, A. Marco Saitta, M. Lazzeri, F. Mauri, C. N. R. Rao, *Phys. Rev. Lett.* **2007**, *99*, 136803.

[99] A. Das, S. Pisana, B. Chakraborty, S. Piscanec, S. K. Saha, U. V. Waghmare, K. S. Novoselov, H. R. Krishnamurthy, A. K. Geim, A. C. Ferrari, A. K. Sood, *Nat. Nanotechnol.* **2008**, *3*, 210.
[100] T. Ando, *J. Phys. Soc. Jpn.* **2006**, *75*, 124701.
[101] S. K. Saha, U. V. Waghmore, H. R. Krishnamurthy, A. K. Sood, *Phys. Rev. B* **2007**, *76*, 201401.
[102] T. Ando, *J. Phys. Soc. Jpn.* **2007**, *76*, 104711.
[103] J. Yan, E. A. Henriksen, P. Kim, A. Pinczuk, *Phys. Rev. Lett.* **2008**, *101*, 136804.
[104] L. M. Malard, D. C. Elias, E. S. Alves, M. A. Pimenta, *Phys. Rev. Lett.* **2008**, *101*, 257401.
[105] A. Das, B. Chakraborty, S. Piscanec, S. Pisana, A. K. Sood, A. C. Ferrari, *Phys. Rev. B* **2009**, *79*, 155417.
[106] B. Das, R. Voggu, C. S. Rout, C. N. R. Rao, *Chem. Commun.* **2008**, 5155.
[107] R. Voggu, B. Das, C. S. Rout, C. N. R. Rao, *J. Phys. Condens. Matter* **2008**, *20*, 472204.
[108] A. K. Manna, S. K. Pati, *Chem. Asian J.* **2009**, *4*, 855.
[109] K. S. Subrahmanyam, R. Voggu, A. Govindaraj, C. N. R. Rao, *Chem. Phys. Lett.* **2009**, *472*, 96.
[110] O. Leenaerts, B. Partoens, F. M. Peeters, *Phys. Rev. B* **2008**, *77*, 125416.
[111] O. Leenaerts, B. Partoens, F. M. Peeters, *Microelectron. J.* **2009**, *40*, 860.
[112] T. O. Wehling, K. S. Novoselov, S. V. Morozov, E. E. Vdovin, M. I. Katsnelson, A. K. Geim, A. I. Lichtenstein, *Nano Lett.* **2008**, *8*, 173.
[113] L. S. Panchakarla, K. S. Subrahmanyam, S. K. Saha, A. Govindaraj, H. R. Krishnamurthy, U. V. Waghmare, C. N. R. Rao, *Adv. Mater.* **2009**, DOI: 10.1002/adma.200901285.
[114] C. N. R. Rao, A. Govindaraj, *Nanotubes and Nanowires (RSC Series on Nanoscience)*, Royal Society of Chemistry, London, **2006**.
[115] *Nanomaterials Chemistry: Recent Developments* (Eds.: C. N. R. Rao, A. K. Cheetham, A. Müller), Wiley-VCH, Weinheim, **2007**.
[116] a) S. Niyogi, E. Bekyarova, M. I. Itkis, J. L. McWilliams, M. A. Hamon, R. C. Haddon, *J. Am. Chem. Soc.* **2006**, *128*, 7720; b) E. Bekyarova, M. E. Itkis, P. Ramesh, C. Berger, M. Sprinkle, W. A. de Heer, R. C. Haddon, *J. Am. Chem. Soc.* **2009**, *131*, 1336; c) K. A. Worsley, P. Ramesh, S. K. Mandal, S. Niyogi, M. E. Itkis, R. C. Haddon, *Chem. Phys. Lett.* **2007**, *445*, 51.
[117] K. S. Subrahmanyam, A. Ghosh, A. Gomathi, A. Govindaraj, C. N. R. Rao, *Nanosci. Nanotechnol. Lett.* **2009**, *1*, 28.
[118] Z. Liu, J. T. Robinson, X. Sun, H. Dai, *J. Am. Chem. Soc.* **2008**, *130*, 10876.
[119] J. R. Lomeda, C. D. Doyle, D. V. Kosynkin, W.-F. Hwang, J. M. Tour, *J. Am. Chem. Soc.* **2008**, *130*, 16201.
[120] a) S. Park, J. An, R. D. Piner, I. Jung, D. Yang, A. Velamakanni, S. T. Nguyen, R. S. Ruoff, *Chem. Mater.* **2008**, *20*, 6592; b) R. Hao, W. Qian, L. Zhang, Y. Hou, *Chem. Commun.* **2008**, 6576; c) Y. Si, E. T. Samulski, *Nano Lett.* **2008**, *8*, 1679.
[121] S. Ryu, M. Y. Han, J. Maultzsch, T. F. Heinz, P. Kim, M. L. Steigerwald, L. E. Brus, *Nano Lett.* **2008**, *8*, 4597.
[122] S. Chakraborty, W. Guo, R. H. Hauge, W. E. Billups, *Chem. Mater.* **2008**, *20*, 3134.
[123] S. Stankovich, R. D. Piner, S. T. Nguyen, R. S. Ruoff, *Carbon* **2006**, *44*, 3342.
[124] a) Y. Xu, Z. Liu, X. Zhang, Y. Wang, J. Tian, Y. Huang, Y. Ma, X. Zhang, Y. Chen, *Adv. Mater.* **2009**, *21*, 1275; b) N. Liu, F. Luo, H. Wu, Y. Liu, C. Zhang, J. Chen, *Adv. Funct. Mater.* **2008**, *18*, 1518; c) R. S. Sundaram, C. Gomez-Navarro, K. Balasubramanian, M. Burghard, K. Kern, *Adv. Mater.* **2008**, *20*, 3050; d) S. Chakraborty, J. Chattopadhyay, W. Guo, W. E. Billups, *Angew. Chem.* **2007**, *119*, 4570; *Angew. Chem. Int. Ed.* **2007**, *46*, 4486.
[125] D. Konatham, A. Striolo, *Nano Lett.* **2008**, *8*, 4630.
[126] L. Ci, Z. Xu, L. Wang, W. Gao, F. Ding, K. F. Kelly, B. I. Yakobson, P. M. Ajayan, *Nano Res.* **2008**, *1*, 116.
[127] R. Muszynski, B. Seger, P. V. Kamat, *J. Phys. Chem. C* **2008**, *112*, 5263.
[128] K. S. Subrahmanyam, MSc (Eng) Thesis, JNCASR, Bangalore, **2008**.
[129] C. Xu, X. Wang, J. Zhu, *J. Phys. Chem. C* **2008**, *112*, 19841.
[130] N. A. Luechinger, E. K. Athanassiou, W. J. Stark, *Nanotechnology* **2008**, *19*, 445201.
[131] Y. Si, E. T. Samulski, *Chem. Mater.* **2008**, *20*, 6792.
[132] S. S. Datta, D. R. Strachan, S. M. Khamis, A. T. C. Johnson, *Nano Lett.* **2008**, *8*, 1912.
[133] X. Wang, S. M. Tabakman, H. Dai, *J. Am. Chem. Soc.* **2008**, *130*, 8152.
[134] a) C. Xu, X. Wang, J. Zhu, X. Yang, L. Lu, *J. Mater. Chem.* **2008**, *18*, 5625; b) G. Williams, B. Serger, P. V. Kamat, *ACS Nano* **2008**, *2*, 1487.
[135] a) K. Nakada, M. Fujita, G. Dresselhaus, M. S. Dresselhaus, *Phys. Rev. B* **1996**, *54*, 17954; b) K. A. Ritter, J. W. Lyding, *Nat. Mater.* **2009**, *8*, 235.
[136] K. Wakabayashi, M. Fujita, H. Ajiki, M. Sigrist, *Phys. Rev. B* **1999**, *59*, 8271.
[137] T. Enoki, N. Kawatsu, Y. Shibayama, H. Sato, R. Kobori, S. Maruyama, K. Kaneko, *Polyhedron* **2001**, *20*, 1311.
[138] K. Kusakabe, M. Maruyama, *Phys. Rev. B* **2003**, *67*, 092406.
[139] T. Enoki, Y. Kobayashi, *J. Mater. Chem.* **2005**, *15*, 3999.
[140] T. Enoki, K. Takai, *Dalton Trans.* **2008**, 3773.
[141] T. Enoki, Y. Kobayashi, K. Fukui, *Int. Rev. Phys. Chem.* **2007**, *26*, 609.
[142] a) H. Lee, N. Park, Y. Son, S. Han, J. Yu, *Chem. Phys. Lett.* **2004**, *398*, 207; b) K. Harigaya, *J. Phys. Condens. Matter* **2001**, *13*, 1295; c) V. Barone, O. Hod, G. E. Scuseria, *Nano Lett.* **2006**, *6*, 2748; d) Y. W. Son, M. L. Cohen, S. G. Louie, *Nature* **2006**, *444*, 347.
[143] a) S. Bhowmick, V. B. Shenoy, *J. Chem. Phys.* **2008**, *128*, 244717; b) O. V. Yazyev, *Phys. Rev. Lett.* **2008**, *101*, 037203.
[144] D. Yu, E. M. Lupton, H. J. Gao, C. Zhang, F. Liu, *Nano Res.* **2008**, *1*, 497.
[145] Y. Wang, Y. Huang, Y. Song, X. Zhang, Y. Ma, J. Liang, Y. Chen, *Nano Lett.* **2009**, *9*, 220.
[146] K. Takahara, K. Takai, T. Enoki, K. Sugihara, *Phys. Rev. B* **2007**, *76*, 035442.
[147] H. S. S. R. Matte, K. S. Subrahmanyam, C. N. R. Rao, *J. Phys. Chem. C* **2009**, *113*, 9982.
[148] S. Wang, P.-J. Chia, L.-L. Chua, L.-H. Zhao, R.-Q. Png, S. Sivaramakrishnan, M. Zhou, R. G.-S. Goh, R. H. Friend, A. T.-S. Wee, P. K.-H. Ho, *Adv. Mater.* **2008**, *20*, 3440.
[149] a) G. Gu, S. Nie, R. M. Feenstra, R. P. Devaty, W. J. Choyke, W. K. Chan, M. G. Kane, *Appl. Phys. Lett.* **2007**, *90*, 253507; b) Z. Chen, Y. Lin, M. J. Rooks, P. Avouris, *Physica E* **2007**, *40*, 228.
[150] X. Li, X. Wang, L. Zhang, S. Lee, H. Dai, *Science* **2008**, *319*, 1229.
[151] X. Wang, Y. Ouyang, X. Li, H. Wang, J. Guo, H. Dai, *Phys. Rev. Lett.* **2008**, *100*, 206803.
[152] I. Meric, M. Y. Han, A. F. Young, B. Ozyilmaz, P. Kim, K. L. Shepard, *Nat. Nanotechnol.* **2008**, *3*, 654.
[153] A. Vollmer, X. L. Feng, X. Wang, L. J. Zhi, K. Müllen, N. Koch, J. P. Rabe, *Appl. Phys. A* **2009**, *94*, 1.
[154] D. C. Elias, R. R. Nair, T. M. G. Mohiuddin, S. V. Morozov, P. Blake, M. P. Halsall, A. C. Ferrari, D. W. Boukhvalov, M. I. Katsnelson, A. K. Geim, K. S. Novoselov, *Science* **2009**, *323*, 610.
[155] K. F. Mak, M. Y. Sfeir, Y. Wu, C. H. Lui, J. A. Misewich, T. F. Heinz, *Phys. Rev. Lett.* **2008**, *101*, 196405.
[156] W. Y. Kim, K. S. Kim, *Nat. Nanotechnol.* **2008**, *3*, 408.

[157] A. A. Balandin, S. Ghosh, W. Bao, I. Calizo, D. Teweldebrhan, F. Miao, C. N. Lau, *Nano Lett.* **2008**, *8*, 902.
[158] H. B. Heersche, P. J. Herrero, J. B. Oostinga, L. M. K. Vandersypen, A. F. Morpurgo, *Nature* **2007**, *446*, 56.
[159] Q. Liang, J. Dong, *Nanotechnology* **2008**, *19*, 355706.
[160] M. Suzuki, I. S. Suzuki, J. Walter, *J. Phys. Condens. Matter* **2004**, *16*, 903.
[161] S. R. C. Vivekchand, C. S. Rout, K. S. Subrahmanyam, A. Govindaraj, C. N. R. Rao, *J. Chem. Sci.* **2008**, *120*, 9.
[162] H. Li, Y. Wang, C. Wang, Y. Xia, *J. Power Sources* **2008**, *185*, 1557.
[163] M. D. Stoller, S. Park, Y. Zhu, J. An, R. S. Ruoff, *Nano Lett.* **2008**, *8*, 3498.
[164] E. Yoo, J. Kim, E. Hosono, H. Zhou, T. Kudo, I. Honma, *Nano Lett.* **2008**, *8*, 2277.
[165] Z. Liu, Q. Liu, Y. Huang, Y. Ma, S. Yin, X. Zhang, W. Sun, Y. Chen, *Adv. Mater.* **2008**, *20*, 3924.
[166] P. Blake, P. D. Brimicombe, R. R. Nair, T. J. Booth, D. Jiang, F. Schedin, L. A. Ponomarenko, S. V. Morozov, H. F. Gleeson, E. W. Hill, A. K. Geim, K. S. Novoselov, *Nano Lett.* **2008**, *8*, 1704.
[167] a) X. Wang, L. Zhi, N. Tsao, Z. Tomovic, J. Li, K. Müllen, *Angew. Chem.* **2008**, *120*, 3032; *Angew. Chem. Int. Ed.* **2008**, *47*, 2990; b) Q. Liu, Z. Liu, X. Zhang, L. Yang, N. Zhang, G. Pan, S. Yin, Y. Chen, J. Wei, *Adv. Funct. Mater.* **2009**, *19*, 894.
[168] A. Peigney, C. Laurent, E. Flahaut, R. R. Bacsa, A. Rousset, *Carbon* **2001**, *39*, 507.
[169] A. Ghosh, K. S. Subrahmanyam, K. S. Krishna, S. Datta, A. Govindaraj, S. K. Pati, C. N. R. Rao, *J. Phys. Chem. C* **2008**, *112*, 15704.
[170] G. Gundiah, A. Govindaraj, N. Rajalakshmi, K. S. Dhathathreyan, C. N. R. Rao, *J. Mater. Chem.* **2003**, *13*, 209.
[171] D. J. Collins, H. C. Zhou, *J. Mater. Chem.* **2007**, *17*, 3154.
[172] B. Huang, Z. Li, Z. Liu, G. Zhou, S. Hao, J. Wu, B. Gu, W. Duan, *J. Phys. Chem. C* **2008**, *112*, 13443.
[173] F. Schedin, A. K. Geim, S. V. Morozov, E. W. Hill, P. Blake, M. I. Katsnelson, K. S. Novoselov, *Nat. Mater.* **2007**, *6*, 652.
[174] N. L. Rangel, J. M. Seminario, *J. Phys. Chem. A* **2008**, *112*, 13699.
[175] J. T. Robinson, F. K. Perkins, E. S. Snow, Z. Wei, P. E. Sheehan, *Nano Lett.* **2008**, *8*, 3137.
[176] J. D. Fowler, M. J. Allen, V. C. Tung, Y. Yang, R. B. Kaner, B. H. Weiller, *ACS Nano* **2009**, *3*, 301.
[177] Z. M. Ao, J. Yang, S. Li, Q. Jiang, *Chem. Phys. Lett.* **2008**, *461*, 276.
[178] A. Ghosh, D. Late, L. S. Panchakarla, A. Govindaraj, C. N. R. Rao, *arXiv.org e-Print Arch. Condens. Matter* **2008**, arXiv:0905.2852v1.
[179] N. Mohanty, V. Berry, *Nano Lett.* **2008**, *8*, 4469.
[180] R. Arsat, M. Breedon, M. Shafiei, P. G. Spizziri, S. Gilje, R. B. Kaner, K. Kalantar-zadeh, W. Wlodarski, *Chem. Phys. Lett.* **2009**, *467*, 344.
[181] A. Sakhaee-Pour, M. T. Ahmadiana, A. Vafai, *Solid State Commun.* **2008**, *145*, 168.
[182] a) J. Lu, I. Do, L. T. Drzal, R. M. Worden, I. Lee, *ACS Nano* **2008**, *2*, 1825; b) C. Shan, H. Yang, J. Song, D. Han, A. Ivaska, L. Niu, *Anal. Chem.* **2009**, *81*, 2378; c) P. K. Ang, W. Chen, A. T. S. Wee, K. P. Loh, *J. Am. Chem. Soc.* **2008**, *130*, 14392.
[183] N. Varghese, U. Mogera, A. Govindaraj, A. Das, P. K. Maiti, A. K. Sood, C. N. R. Rao, *ChemPhysChem* **2009**, *10*, 206.
[184] a) B. Z. Jang, A. Zhamu, *J. Mater. Sci.* **2008**, *43*, 5092; b) J. J. Mack, L. M. Viculis, A. A. R. Luoh, G. Yang, H. T. Hahn, F. K. Ko, R. B. Kaner, *Adv. Mater.* **2005**, *17*, 77.
[185] P. K. Hansma, P. J. Turnerl, R. S. Ruoff, *Nanotechnology* **2007**, *18*, 044026.
[186] T. Ramanathan, A. A. Abdala, S. Stankovich, D. A. Dikin, M. H. Alonso, R. D. Piner, D. H. Adamson, H. C. Schniepp, X. Chen, R. S. Ruoff, S. T. Nguyen, I. A. Aksay, R. K. Prud' Homme, L. C. Brinson, *Nat. Nanotechnol.* **2008**, *3*, 327.
[187] B. Das, K. E. Prasad, U. Ramamurty, C. N. R. Rao, *Nanotechnology* **2009**, *20*, 125705.
[188] A. Yu, P. Ramesh, M. E. Itkis, E. Bekyarova, R. C. Haddon, *J. Phys. Chem. C* **2007**, *111*, 7565.
[189] X. Zhang, Y. Huang, Y. Wang, Y. Ma, Z. Liu, Y. Chen, *Carbon* **2008**, *47*, 313.
[190] T. J. Booth, P. Blake, R. R. Nair, D. Jiang, E. W. Hill, U. Bangert, A. Bleloch, M. Gass, K. S. Novoselov, M. I. Katsnelson, A. K. Geim, *Nano Lett.* **2008**, *8*, 2442.
[191] A. Sakhaee-Pour, *Solid State Commun.* **2009**, *149*, 91.
[192] N. A. Luechinger, N. Booth, G. Heness, S. Bandyopadhyay, R. N. Grass, W. J. Stark, *Adv. Mater.* **2008**, *20*, 3044.
[193] S. Watcharotone, D. A. Dikin, S. Stankovich, R. Piner, I. Jung, G. H. B. Dommett, G. Evmenenko, S. Wu, S. Chen, C. Liu, S. T. Nguyen, R. S. Ruoff, *Nano Lett.* **2007**, *7*, 1888.
[194] H. Chen, M. B. Muller, K. J. Gilmore, G. G. Wallace, D. Li, *Adv. Mater.* **2008**, *20*, 3557.
[195] A. Kara, C. Leandri, M. E. Davila, P. de Padova, B. Ealet, H. Ougaddou, B. Aufray, G. L. Lay, *arXiv.org e-Print Arch. Condens. Matter* **2008**, arXiv:0811.2611v1.
[196] E. F. Sheka, *arXiv.org e-Print Arch. Condens. Matter* **2009**, arXiv:0901.3663.